MULTIUSER DETECTION IN CDMA USING BLIND TECHNIQUES

A Thesis Submitted to
the Graduate School of Engineering and Sciences of
İzmir Institute of Technology
in Partial Fulfillment of the Requirements for the Degree of

MASTER OF SCIENCE

in Electrical and Electronics Engineering

by
Eşref Olgu ALTINSOY

October 2004
İZMİR

We approve the thesis of **Eşref Olgu ALTINSOY**

Date of Signature

..... **26.10.2004**

Asst. Prof. Dr. Mustafa Aziz ALTINKAYA

Supervisor

Department of Electrical and Electronics Engineering

İzmir Institute of Technology

..... **26.10.2004**

Asst. Prof. Dr. Serdar ÖZEN

Department of Electrical and Electronics Engineering

İzmir Institute of Technology

..... **26.10.2004**

Asst. Prof. Dr. Reyat YILMAZ

Department of Electrical and Electronics Engineering

Dokuz Eylül University

..... **26.10.2004**

Prof. Dr. F. Acar SAVACI

Head of Department

İzmir Institute of Technology

ACKNOWLEDGMENTS

I would like to express my special thanks to my supervisor Asst. Prof. Dr. Mustafa Aziz Altınkaya for his guidance and help throughout my research.

I would also like to thank my thesis committee members Asst. Prof. Dr. Serdar Özen and Asst. Prof. Dr. Reyat Yılmaz for their advice and comments on this study.

Moreover, I wish to thank to my friends Olcay Kalkan, Osman Akın, and Emel Karagöz for their help and support throughout my work, and also for their understanding.

Finally, special thanks to my family for their support, understanding, and encouragement for years.

ABSTRACT

In code division multiple access (CDMA) systems, blind multiuser detection (MUD) techniques are of great importance, especially for downlinks, since in practice, it may be unrealistic for a mobile user to know the spreading codes of other active users in the channel. Furthermore, blind methods remove the need for training sequences which leads to a gain in the channel bandwidth.

Subspace concept in blind MUD is an alternative process to classical and batch blind MUD techniques based on principle component analysis, or independent component analysis (ICA) and ICA-like algorithms, such as joint approximate diagonalization of eigen-matrices (JADE), blind source separation algorithm with reference system, etc. Briefly, the desired signal is searched in the signal subspace instead of the whole space, in this type of detectors.

A variation of the subspace-based MUD is reduced-rank MUD in which a smaller subspace of the signal subspace is tracked where the desired signal is contained in. This latter method leads to a performance gain compared to a standard subspace method.

In this thesis, blind signal subspace and reduced-rank MUD techniques are investigated, and applied to minimum mean square error (MMSE) detectors with two different iterative subspace tracking algorithms. The performances of these detectors are compared in different scenarios for additive white Gaussian noise and for multipath fading channels as well. With simulation results the superiority of the reduced-rank detector to the signal subspace detector is shown. Additionally, as a new remark for both detectors, it is shown that, using minimum description length criterion in subspace tracking algorithm results in an increase in rank-tracking ability and correspondingly in the final performance. Finally, the performances of these two detectors are compared with MMSE, adaptive MMSE and JADE detectors.

ÖZET

Kod bölüşümlü çoklu erişim (code division multiple access, CDMA) gezgin iletişim uygulamalarında, özellikle baz istasyonundan gezgin kullanıcı yönüne iletimde; kullanıcının, kanaldaki diğer kullanıcıları ve bunlara ait imza kodları gibi bilgileri edinmesi güç bir işlem olduğundan CDMA uygulamalarında, gözü kapalı çok kullanıcılı sezim teknikleri zaman içerisinde önem kazanmıştır. Bunun yanında, gözü kapalı teknikler öncül (pilot) dizi ihtiyacını ortadan kaldırdıklarından dolayı band genişliğinde bir miktar kazanç da sağlar.

Gözü kapalı çok kullanıcılı sezimde altuzay yaklaşımı, diğer geleneksel ve verinin tümünü birden işleyen, ana bileşen çözümlemesi veya bağımsız bileşen çözümlemesi (independent component analysis, ICA) yöntemleri üzerine kurulu ya da özmatrislerin birleşik yaklaşık köşegenleştirilmesi (joint approximate diagonalization of eigen-matrices, JADE) ve başvuru sistemli gözü kapalı kaynak ayrıştırma işlemyolu gibi ICA benzeri yöntemleri kullanan gözü kapalı tekniklere karşı bir seçenek oluşturmaktadır. Özetlemek gerekirse, altuzay yaklaşımı kullanan alıcılarda, ilgili kullanıcıya ait işaret bütün sinyal uzayı yerine sinyal uzayının bir altuzayında aranır.

Altuzay yaklaşımının bir türevi de ilgili kullanıcıya ait işaretin de içinde yer alacağı, sinyal altuzayının daha küçük boyutlu bir altuzayının aranması anlamına gelen indirgenmiş boyutlu çok kullanıcılı sezimdir. Bu indirgenmiş boyut yöntemi, standart bir altuzay yöntemiyle karşılaştırıldığında ek bir başarım kazancı sağlar.

Bu tezde, gözü kapalı sinyal altuzayı ve indirgenmiş boyutlu çok kullanıcılı sezim yöntemleri incelenerek, iki farklı altuzay yakalama işlemyolu kullanılarak en küçük ortalama karesel hata (minimum mean-square error, MMSE) alıcılarına uygulanmakta ve bu alıcıların başarım çözümlemeleri farklı sistem senaryolarıyla, toplanır beyaz Gauss gürültü ve çok yollu sönümlemeli kanallar için karşılaştırılmaktadır. Benzetim sonuçlarıyla, indirgenmiş boyutlu sezicinin sinyal altuzayı sezicisine göre başarım üstünlüğü gösterilmiştir. Ayrıca, her iki alıcı için söylenebilecek yeni bir durum olarak; altuzay yakalama işlemyolunda, ölçüt olarak en küçük betimleme uzunluğu yaklaşımı kullanılmasının, hem altuzayın boyutunu yakalama yeteneğinde hem de sezim başarımında ek bir artışa sebep olduğu gösterilmiştir. Bunlara ek olarak, bu iki alıcının hata başarımı, MMSE, uyarlamalı MMSE ve JADE alıcılarıyla da karşılaştırılmıştır.

To my family

TABLE OF CONTENTS

LIST OF FIGURES

LIST OF TABLES

LIST OF ABBREVIATIONS

CDMA	Code Division Multiple Access
WCDMA	Wide-Band Code Division Multiple Access
UMTS	Universal Mobile Telecommunications System
UWC	Universal Wireless Communications
GPRS	General Packet Radio System
PCS	Personal Communications Systems
SMS	Short Messaging Services
AMPS	Advanced Mobile Phone Service
EDGE	Enhanced Data Rates for Global Evolution
TDMA	Time Division Multiple Access
FDMA	Frequency Division Multiple Access
GSM	Global System for Mobile Communications
3G	Third Generation
SS	Spread Spectrum
DS-SS	Direct Sequence Spread Spectrum
FH-SS	Frequency Hopping Spread Spectrum
TH-SS	Time Hopping Spread Spectrum
LPI	Low Probability of Intercept
AJ	Anti-Jamming
PN	Pseudo-Noise
MUD	Multiuser Detection
SUD	Single User Detection
MAI	Multiple Access Interference
MSE	Mean-Square Error
MMSE	Minimum Mean-Square Error
MOE	Mean Output Energy
BSS	Blind Source Separation
ICA	Independent Component Analysis
JADE	Joint Approximate Diagonalization of Eigen-Matrices
SVD	Singular Value Decomposition
ED	Eigen-Value Decomposition

AIC	Akaike Information Criterion
MDL	Minimum Description Length
PAST	Projection Approximation Subspace Tracking
LORAF	Low-Rank Adaptive Filters
AWGN	Additive White Gaussian Noise
SIR	Signal-to-Interference Ratio
SNR	Signal-to-Noise Ratio

CHAPTER 1

INTRODUCTION

The increasing demands in wireless personal and mobile communication systems both to provide and accommodate high quality voice services and other multirate services such as internet access from hand-held mobile terminals, also increased the interest in code division multiple access (CDMA) because it provides high-frequency usage and it is suitable for multimedia and multirate services. As a result, CDMA was chosen to be the main multiple access scheme of 3rd generation (3G) wireless and cellular systems. Consequently, there has been an accelerated interest in finding better multiuser detection (MUD) techniques which provide superior performance with respect to single user detection (SUD) techniques but require higher computational complexity.

In this thesis, subspace-based blind MUD schemes of CDMA are investigated. The emphasized methods may be preferable to other batch methods since they work in a sample-by-sample fashion adaptively without requiring the whole data for performing the detection.

After this introductory chapter, Chapter 2 discusses briefly the history of mobile communication systems till 3G systems. Furthermore, CDMA concept from the perspective of both spread spectrum (SS) and multiple access systems is introduced. At the end of Chapter 2, some basic definitions for CDMA are given, and also CDMA signal models both in synchronous and asynchronous channels and matched filter are defined.

In Chapter 3, several detector schemes are discussed beginning from single-user detector to adaptive multiuser detectors with different requirements for each detector. Some performance criteria are also defined here. At the end of this chapter, performance comparisons of all the considered methods are given with simulation results.

Chapter 4 is the section where blind MUD concept is studied. The batch type algorithm, joint approximate diagonalization of eigen-matrices (JADE) is introduced as an example for ICA-class BSS techniques, at the beginning. Then, subspace approach in blind MUD is presented and two such detectors rank-K and reduced-rank detectors are derived. Additionally, performances of these detectors and their comparison by simulation results for several channel conditions are given in this chapter.

Finally, Chapter 5 includes some conclusion remarks and suggestions for future studies.

CHAPTER 2

THE EVOLUTION PATH OF MOBILE COMMUNICATIONS TOWARDS SPREAD SPECTRUM SYSTEMS

In this chapter, the evolution of mobile communication systems are mentioned starting with the earliest systems employed in 1940's and coming to spread spectrum systems which are adopted as the main multiple access schemes of 3G mobile communication systems. Firstly, a brief historical account of mobile communication systems will be given.

History of today's mobile communications goes back till mid-1940s, to a domestic public service operating at 150 MHz with only three channels. Development from a domestic use to the use of entire world is summarized in Table 2.1 [3] through the important steps, chronologically.

2.1 Evolution to 3rd Generation (3G) Systems

Time division multiple access (TDMA) system which is based on the standards IS-54 [9] and its evolved version IS-136 [10] developed by Telecommunications Industry Association (TIA) and Electronics Industry Association (EIA), Global System for Mobile Communications (GSM) [11, 12] and also cdmaOne which is based on the standard IS-95 [13] developed by TIA and EIA may be referred to as 2nd generation (2G) mobile systems. Firstly, let's have a look at those systems.

2.1.1 TDMA (IS-136)

TDMA as a mobile network, designed with IS-54 and later with IS-136, provide a communication scheme where data from multiple users is time-division multiplexed using a number of time slots and sent out over a physical channel. Since each time slot used may be assigned to a different user, the capacity is increased in the same proportion. Based on this concept, first IS-54, then a newer version IS-136 is designed as a TDMA standard by TIA and EIA. According to these standards a TDMA frame is 40 ms long and consists of 6 slots each 6.67 ms. Features for IS-136 system is given in Appendix A.

Table 2.1: Chronology of important developments in mobile communications [3]

1946	First domestic public land mobile service introduced in St.Louis. The system operated at 150 MHz and had only three channels.
1956	First use of a 450 MHz system. Users had to use a push-to-talk button and always needed operator assistance.
1964	First, automatic system, called MJ. It operated at 150 MHz and could select channels automatically. However, roaming was operator-assisted.
1969	First MK system. Like the MJ system, it was automatic, but worked at 450 MHz bands.
1970	Federal Communication Commission (FCC) sets aside 75 MHz for high-capacity mobile telecom systems.
1974	FCC grants common carriers 40 MHz for development of cellular systems.
1978	First cellular system called Advanced Mobile Phone Service (AMPS) was introduced in Chicago on a trial basis.
1981	Cellular systems deployed in Europe.
1983	First commercial deployment of a cellular system in Chicago. It was an analog system and did not have a user data transport capability. Analog systems around 450 and 900 MHz band were also introduced in many countries of Europe during 1981 - 1990.
1989	FCC grants another 10 MHz bandwidth for cellular systems, thus giving a total of 50 MHz
1991	GSM was introduced in Europe and other countries of the world.
1993	TDMA system called IS-54 was introduced in US. Short Messaging Services (SMS) available in GSM.
1995	CDMA cellular and Personal Communications Systems (PCS) technology was introduced in US.
1997	General Packet Radio System (GPRS) standards were published.
1999	Standards for 3G wireless services were published.

2.1.2 GSM

Cellular mobile telephony was first introduced in Sweden, Norway, Finland, and Denmark in Europe in 1981, as analog systems operating around 450 and 900 MHz bands. In a few years, other European countries also installed such systems. But those systems were not compatible with each other, and thus inter-system communications were not possible. To overcome this problem, a standard was introduced in 1990, called Global System for Mobile Communications (GSM) that uses 2 frequency bands around 900 MHz where the first band operates at 890 to 915 MHz as the reverse link (uplink) and the second band, forward link (downlink) at 935 to 960 MHz. Here, the reverse link corresponds to the communication from the mobile user to the base station and the forward link to the communication in the opposite direction.

In GSM each physical channel has a bandwidth of 200 kHz and consists of 8 time slots, each assigned to a different user. In GSM, the length of a TDMA frame is 4.625

ms. Some more detailed features of GSM is given in Appendix B [3].

2.1.3 cdmaOne (IS-95)

cdmaOne was demonstrated in 1998 as an application of spread spectrum technology to a mobile communication system. According to this scheme each user is assigned a unique pseudo-noise (PN) code whose clock rate (chip rate) is generally much higher than the user data rate. The specifications of cdmaOne is defined by IS-95. In Appendix C [3], you may see the features of cdmaOne.

2.1.4 3G Systems

The growing mobile services and the additional needs built up the 3G systems. We may classify the following four systems as 3G mobile systems, they are: cdma2000, Universal Wireless Communications (UWC-136), wide-band code division multiple access with frequency division duplex (WCDMA-FDD), and wide-band code division multiple access with time division duplex (WCDMA-TDD). Since WCDMA is widely known as Universal Mobile Telecommunications System (UMTS) in Europe, these last two systems are also called as UMTS-FDD and UMTS-TDD, respectively. The evolution path to 3G systems is illustrated in Figure 2.1 [3].

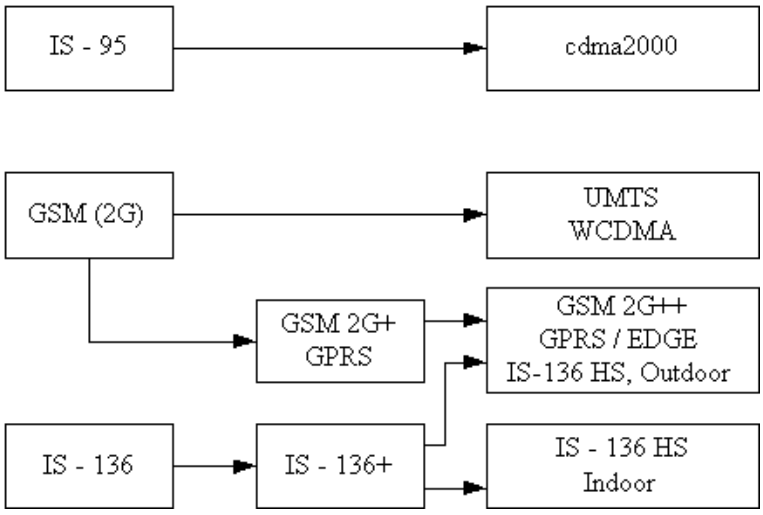

Figure 2.1: The Evolution Path to 3G Systems

cdma2000 is actually an evolution of cdmaOne. It is a direct sequence spread spectrum system and may use one or more carriers, and operates in FDD mode.

UWC-136 may be called as the TDMA version of 3G systems for use in North America. Evolution to UWC-136 corresponds to the path of IS-136 evolution in Figure 2.1

WCDMA (UMTS as called in Europe, also called UMTS Terrestrial Radio Access (UTRA)), uses a direct sequence spread spectrum signal with a 5 MHz bandwidth and operates both in FDD and TDD modes. As seen in Figure 2.1 standards have designed UMTS to use the core networks of GSM and similarly the packet mode data services of UMTS have been harmonized with general packet radio system (GPRS), which is a packet data service capability of GSM. Additionally, a standard called Enhanced Data Rates for GSM Evolution (EDGE) has been defined in order to support internet protocol (IP) based services in GSM at rates up to 384 kb/s. EDGE (also called as Enhanced Data Rates for Global Evolution) is a cost-efficient upgrade to existing GSM/GPRS and TDMA networks. It operates in existing spectra and increases the speed over the air interface by introducing a more advanced coding scheme where every time slot can transport more data [14].

2.2 Spread Spectrum Communication Systems

Spread Spectrum (SS) has its origin in the military area resulting from two basic necessities in military communications.One of them is the need for a reliable communication and the second one is the need for a system resistant against jamming. These two

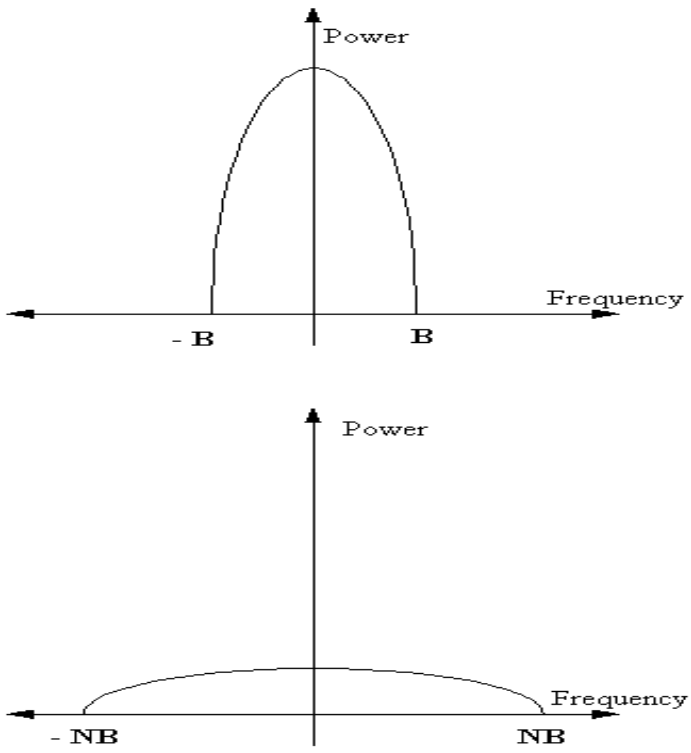

Figure 2.2: Spectrum of SS signal where N is the spreading factor.

necessities also represent the two basic superiorities of SS communication systems; low

probability of intercept (LPI) and antijam (AJ) capability.

SS is a communication technique where the transmitted signal is increased in bandwidth (spreading) at the transmitter and then decreased in bandwidth (despreading) again by the same amount at the receiver. This bandwidth spreading operation makes the transmitted signal appear similar to random noise in the channel as in Figure 2.2 and difficult to be detected and demodulated by receivers other than the intended ones, and so, neither jammed nor exploited in any manner.

There are several SS techniques in practice. Direct sequence (DS-SS) and frequency hopping (FH-SS) are the two most popular ones. As shown in Figure 2.3, a rarely preferred technique when compared to the previous two is time hopping (TH-SS), and there are other hybrid techniques which blend mentioned SS techniques together.

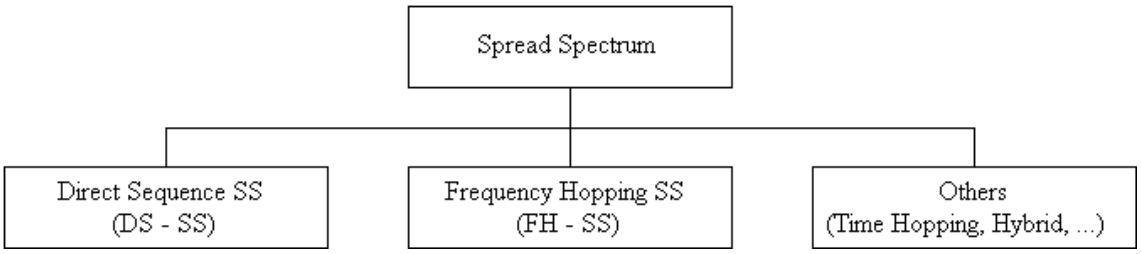

Figure 2.3: Types of SS communication system

2.2.1 Direct Sequence Spread Spectrum (DS-SS)

DS is the best known SS technique. A DS-SS signal *c(t)* is formed by linearly modulating the output sequence $\{c_n\}$ of a pseudo-random number generator by a train of pulses of duration T_c called the chip duration. The word *chip* stands for the time it takes to transmit one bit of a pseudo-noise (PN) sequence. The PN sequence may be formulated as

$$c(t) = \sum_{n=-\infty}^{\infty} c_n p(t - nT_c) \tag{2.1}$$

where *p(t)* is the basic rectangular pulse shape. Figure 2.4 gives a block diagram of the DS-SS system.

In a DS-SS system an already modulated signal is modulated second time to produce a data sequence, occupying a bandwidth in excess of the minimum necessary one to send it. The spectrum spreading is done just before transmission, through the use of a pseudo-random number sequence, mentioned above, that is independent of the data

sequence. Pseudo-randomness of this sequence is important in design of DS-SS signals.

Since the generation of PN codes is relatively easy, it is also easy to introduce a large processing gain in DS-SS systems. It may be thought that the despreading

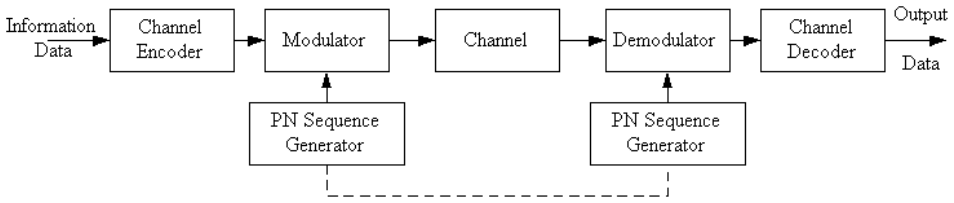

Figure 2.4: Block diagram of a DS-SS system [1]

operation is the same as the spreading operation because the signal is multiplied with the corresponding PN code both at the transmitter and the receiver. Therefore, as it is illustrated in Figure 2.5, the information signal is despread while possible jamming signals in the channel are spread before data detection is performed. So jamming effects are reduced.

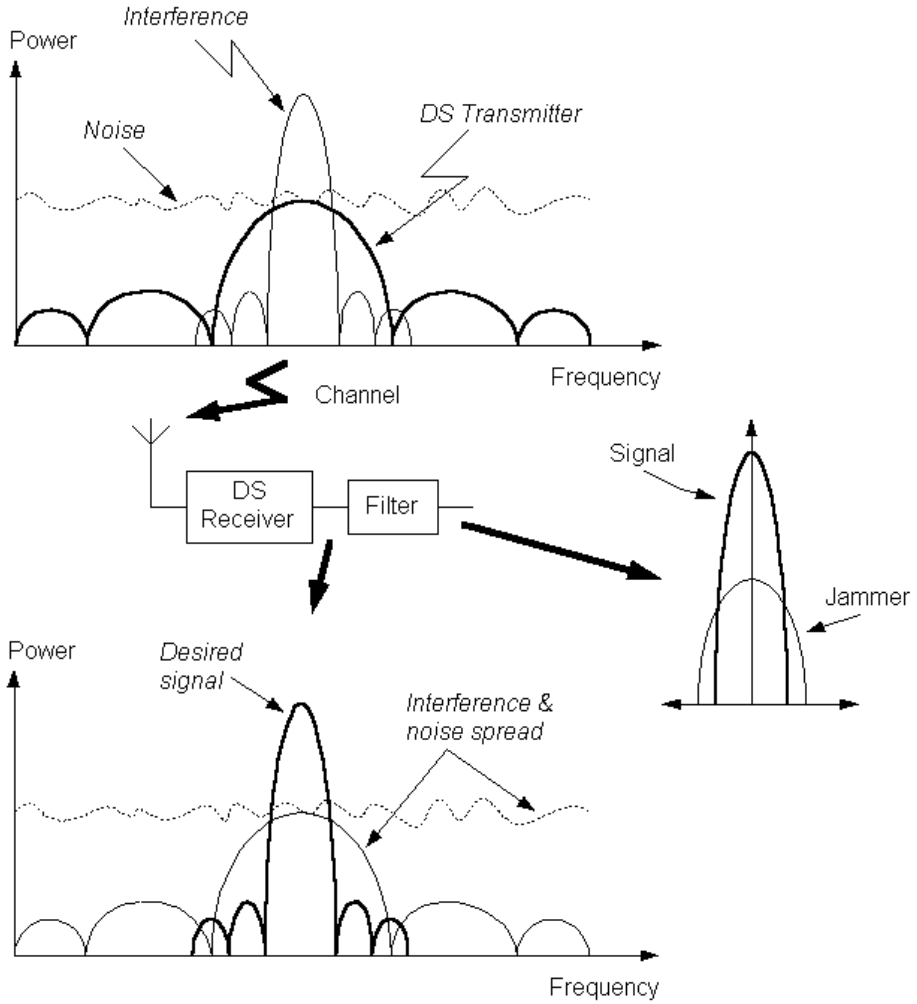

Figure 2.5: Anti-jamming (AJ) property of DS-SS system

The main problem in applying DS is the so-called near-far effect which is illustrated

in Figure 2.6. This effect is present when an interfering signal is much closer to the receiver than the intended signal. Although the cross-correlation between codes A and B is low, the correlation between the received signal from the interfering user and code A can be higher than the correlation between the received signal from the intended transmitter and code A. The result is that proper data detection is not possible [15]. Near-far effect is an important criteria in multiuser detector design.

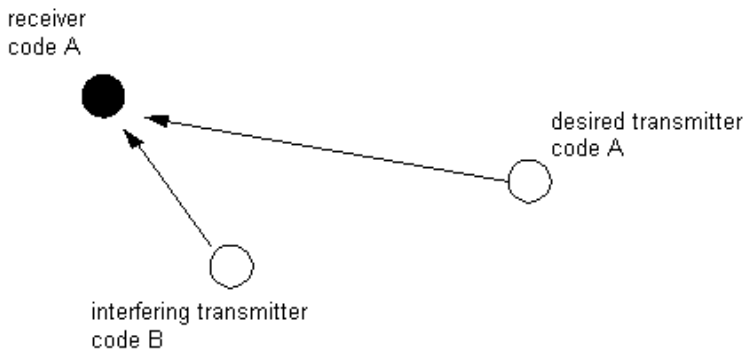

Figure 2.6: Near-Far Effect

2.2.2 Frequency Hopping Spread Spectrum (FH-SS)

In FH-SS the pseudo-random number sequence is used to select the frequency of the transmitted signal pseudo-randomly among the possible frequencies in SS bandwidth. An FH-SS signal *c(t)* is formed by nonlinearly modulating a train of pulses with a sequence of pseudo-randomly generated frequency shifts $\{f_n\}$.

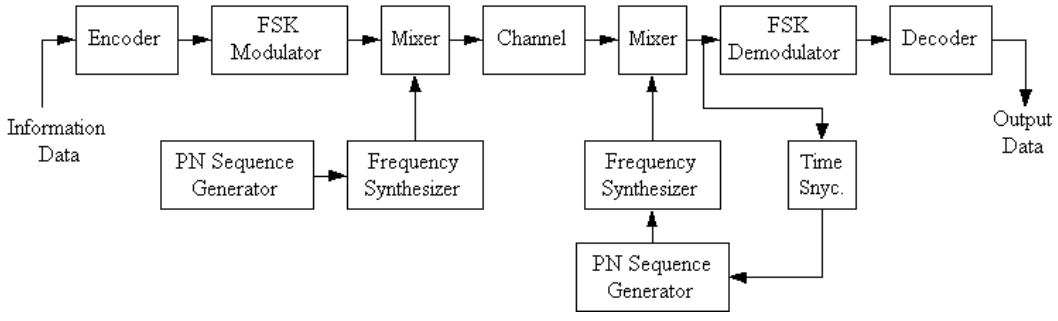

Figure 2.7: Block diagram of an FH-SS system [1]

Mathematically, it is

$$c(t) = \sum_{n=-\infty}^{\infty} \exp\{j(2\pi f_n + \phi_n)\} p(t - nT_h) \tag{2.2}$$

where *p(t)* is again the basic rectangular pulse shape of duration T_h, the hop time, and

$\{\phi_n\}$ is a sequence of random phases associated with the generation of the hops. In Figure 2.7, block diagram of an FH-SS system is given. An example of an FH-SS pattern is illustrated in Figure 2.8.

While applying FH technique, the carrier frequency hops according to a unique sequence of length N. In this way the bandwidth is increased by a factor N, if the channels are non-overlapping. A disadvantage of FH technique as opposed to DS is that obtaining a high processing gain (spreading factor) is hard.

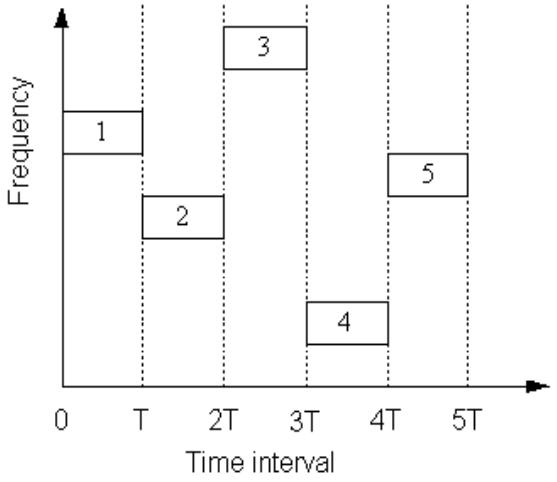

Figure 2.8: An example of an FH-SS pattern

On the other hand, FH is less effected by the near-far effect than DS. FH sequences have only a limited number of hits with each other. This means that if a near-interferer is present, only a number of frequency-hops will be blocked instead of the whole signal. From the hops that are not blocked it should be possible to recover the original data message [15].

2.2.3 Other Spread Spectrum Techniques

Analogous with FH-SS, in TH-SS, a time interval which is much larger than the reciprocal of the information rate is subdivided into a large number time slots. The coded information symbols are transmitted in a pseudorandomly selected time slot as a block of one or more code words.

Hybrid type SS systems combine several SS techniques together. The mostly known of such types is represented by DS/FH and combines DS and FH techniques which means that a PN sequence is used in combination with frequency hopping. The signal transmitted on a single hop consists of a DS-SS signal which is demodulated coherently. However, the received signals from different hops are combined noncoherently.

Another possible hybrid SS type is DS/TH that combines DS and TH techniques. This is not as practical as DS/FH, because of an increase in system complexity and more strict timing requirements [1].

2.3 Multiple Access Communication Systems

A multiple access communication system is a system in which several transmitters share a common channel. In such a system the receiver receives a noisy superposition of the signals sent by active transmitters in the system. Multiple access systems are also referred to as multipoint-to-point communication systems as illustrated in Figure 2.9 [16].

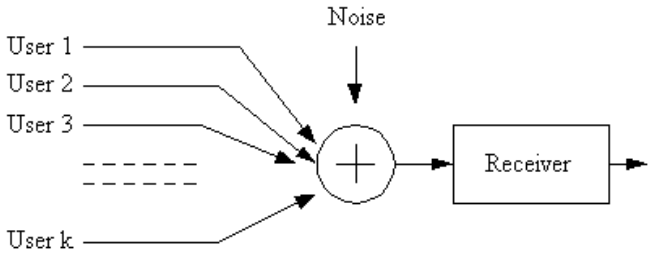

Figure 2.9: Multiple access communication scheme

We may classify some types of multiple access communications as TDMA, FDMA, CDMA, etc.. Figure 2.10 illustrates this classification.

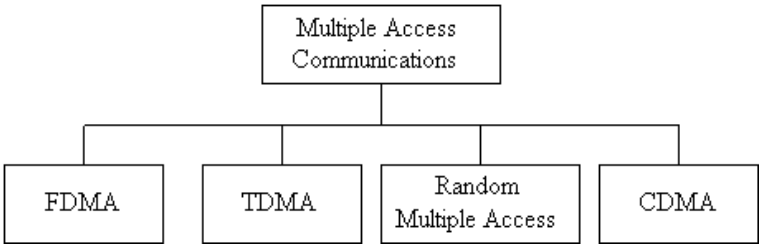

Figure 2.10: Types of multiple access communications

From the perspective of commercial communications, the most popular and important use of SS is a multiple accessing technique, and it is a serious alternative to either frequency division multiple access (FDMA) or time division multiple access (TDMA), referred to as code division multiple access (CDMA).

In TDMA, time is divided into time slots assigned to incoming streams from different users, whereas in FDMA each user is assigned a different carrier frequency in order to prevent their spectrums from overlapping. The ideas of TDMA and FDMA is shown in frequency versus time axis in Figure 2.11.

As we mentioned, CDMA is an alternative to both of these multiple access schemes, FDMA and TDMA. As it is seen in Figure 2.12, each user is assigned a differ-

ent, unique code called signature waveform. All signals occupy the same bandwidth and are transmitted simultaneously in time. As mentioned before, each transmitter sends its information data stream by modulating its uniquely assigned signature waveform as in a single user digital communication system.

Four different and unique codes are seen in Figure 2.12 which are assigned to four different users all are communicating at the same time while sharing the same frequency band.

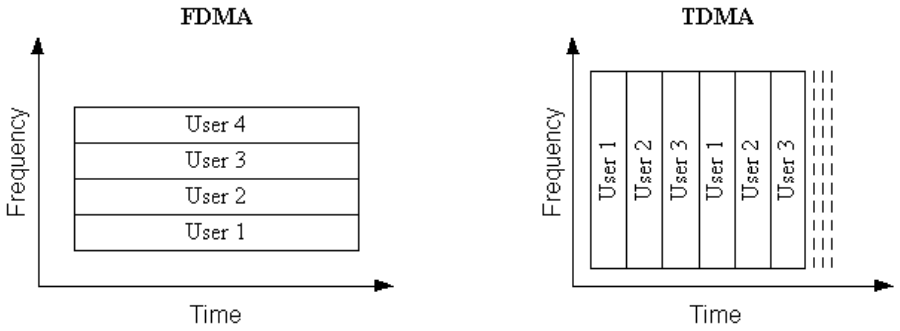

Figure 2.11: FDMA and TDMA

However, as illustrated in Figure 2.11, users are not able to communicate sharing same frequency band in FDMA or sharing time in TDMA.

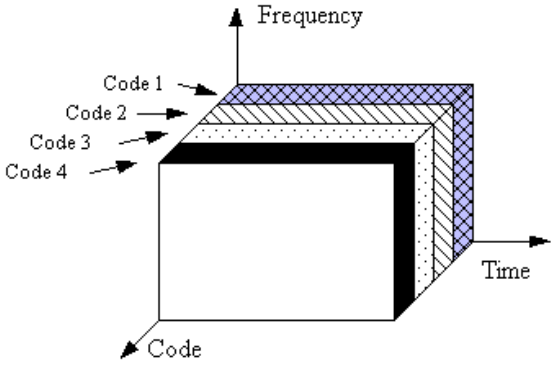

Figure 2.12: Illustration for code assignment in CDMA

2.4 CDMA Basics

Some basic parameters of a CDMA signal may be defined using Figure 2.13. In the figure we see how a two-bit sequence is spread using short codes. The information bits $\{+1, -1\}$ are used to modulate the spreading code (or PN sequence), that is $\{+1, -1, +1, +1, -1, -1, +1\}$, with T_c, chip duration. T is the bit duration. For the second information bit $\{-1\}$, how the PN sequence is inversed is to be noticed.

2.4.1 Processing Gain

Processing gain is a measure that represents how much the bandwidth of the information signal is increased after spreading or analogously how many bits are used to represent a single information bit. Processing gain is also called as the number of chips per symbol, spreading factor, or spreading gain and it is defined as

$$N = 10\ \log_{10}\ (R_c/R_b) = 10\ \log_{10}\ (T_b/T_c)\ \ \text{(dB)}. \tag{2.3}$$

2.4.2 PN-Sequences

PN-sequences are the main elements of a CDMA system. Pseudo-randomness of spreading codes are very important since this property provides them the ability to be regenerated. The receiver detects the signals by means of these spreading codes that are uniquely assigned to each user. So they should be generated using some predefined algorithms. Additionally, in order to provide an easier detection at the receiver, the cross-correlations of these sequences should be small.

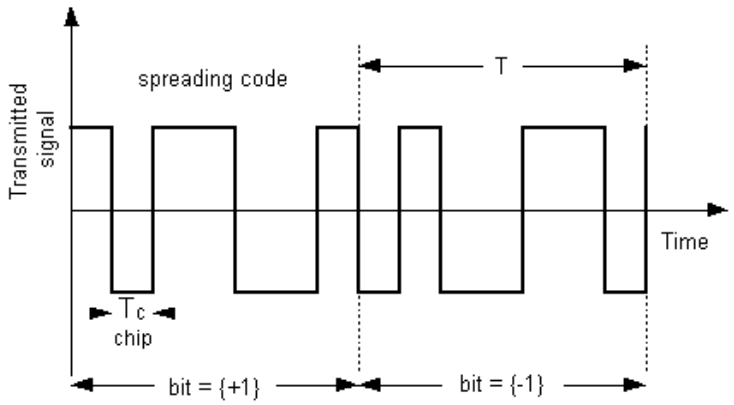

Figure 2.13: An example of spreading

There are several algorithms for generating PN-sequences to be used in CDMA systems. The most preferred ones are maximal length sequences, Gold sequences and Walsh sequences. Next, we will mention properties of those sequences.

2.4.2.1 Maximal Length Sequences

These sequences are generated using shift registers. Shift register sequences having the maximum possible period for an n element shift register are called maximal length sequences or m-sequences. Therefore for a shift register with n elements, the longest or

maximum length sequence which can be generated is $N = 2^n - 1$ [4].

It is defined that a (j, k) linear code C is a k-dimensional subspace of the vector space of all the binary j-tuples where j is the length of the linear block code and $j > k$ [17, 18]. So, we may say that m-sequences are cyclic codes with $(2^n - 1, n)$. That is, an m-sequence code C is a linear code of $(2^n - 1, n)$ and every cyclic shift of a code vector in C is also a code vector in C.

Auto-correlation function of a periodic signal $\omega(t)$ with period T is

$$R_i(\tau) = \frac{1}{T} \int_0^T \omega_i(t)\omega_i(t+\tau)dt \tag{2.4}$$

from where (2.5) is derived as

$$R_i(\tau) = \begin{cases} 1 - \frac{N+1}{NT_c}|\tau| & , \quad |\tau| \leq T_c \\ -\frac{1}{N} & , \quad \text{elsewhere} \end{cases} . \tag{2.5}$$

Auto-correlation defines how much a function correlates with a time shifted version of itself with respect to that time shift. Figure 2.14 shows the periodic auto-correlation function for m-sequences. m-sequences exhibit good auto-correlation properties which is important in CDMA while rejecting multipath interference.

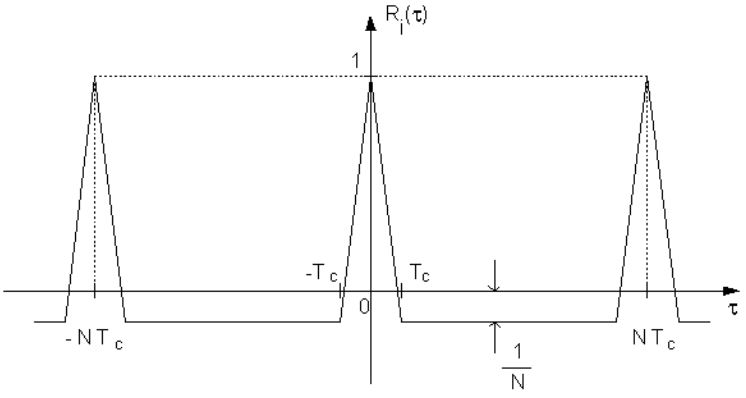

Figure 2.14: Auto-correlation function [2]

Another property that is important in CDMA is the cross-correlation property of these sequences which is expected to be as small as possible since exhibiting small cross-correlations, these codes help receiver to separate the desired signal from other users' signals. However, cross-correlation property of m-sequences is relatively poor which makes m-sequences unsuitable for CDMA. The cross-correlation for periodic signals ω_i and ω_j of period T is defined as

$$C_{ij} = \frac{1}{T}\int_0^T \omega_i(t)\omega_j(t-\tau)dt. \tag{2.6}$$

The cross-correlation values of m-sequences with different number of shift register elements and their comparisons with corresponding Gold code sets are given in Table 2.2. And in Figure 2.15 an example for generating m-sequences of three shift register elements is illustrated.

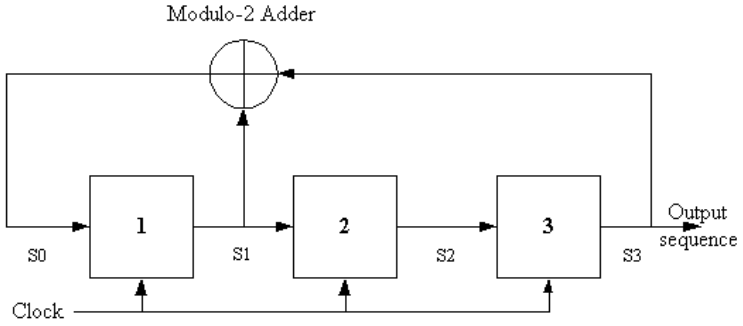

Figure 2.15: An example for generating m-sequences of 3-elements [2]

2.4.2.2 Gold Sequences

Selected pairs of m-sequences exhibit a three valued periodic cross-correlation function with reduced upper bound correlation levels when compared with the rest of the m-sequence set. This subset of m-sequence family is also referred to as the preferred pair and one such unique subset exists for each sequence length. Gold sequences are derived from m-sequences in this manner with better periodic cross-correlation properties. This cross-correlation property of Gold sequences is given in three values with $\{-1, -t(n), t(n)-2\}$ where

$$t(n) = \begin{cases} 2^{(n+1)/2}+1 & , \quad n \text{ odd} \\ 2^{(n+2)/2}+1 & , \quad n \text{ even} \end{cases} . \tag{2.7}$$

Although Gold sequences are derived from m-sequences, Gold sequences are non-linear, while m-sequences remain linear. A Gold sequence generator of 6-elements is given in Figure 2.16.

Table 2.2 compares m-sequences and Gold codes with respect to their set sizes and peak levels where it can be seen that the available set size for m-sequences is very much smaller than the sequence length, N. However, Gold codes are more acceptable than m-sequences due to their set size and peak level properties. Also, in Table 2.3 occurrence frequency of cross-correlations for Gold codes are listed.

2.4.2.3 Walsh Sequences

Walsh Sequences have the attractive property that all codes in a set are orthogonal. A series of codes $w_k(t)$ for $k = 0, 1, 2, ..., N$ are orthogonal with weight N over the interval $0 \leq t \leq T$ when

$$\int_0^T w_n(t)\ w_m(t)\ dt = \begin{cases} N, & \text{for} \quad n = m \\ 0, & \text{for} \quad n \neq m \end{cases} \tag{2.8}$$

where n and m are integers and N is a non-negative constant which does not depend on the indices m and n but only depends on the code length N.

Table 2.2: Comparison of m-sequences and Gold codes with their set sizes and peak levels [4].

		m-sequences		Gold codes	
n	N	set size	peak level	set size	peak level
3	7	2	5	9	5
4	15	2	9	17	9
5	31	6	11	33	9
6	63	6	23	65	17
7	127	18	41	129	17
8	255	16	95	257	33
9	511	48	113	513	33
10	1023	60	383	1025	65
11	2047	176	287	2049	65
12	4095	144	1407	4097	129

Walsh sequence systems are limited to code lengths of $N = 2^n$. When used in communication systems the code length N enables N orthogonal codes to be obtained.

Table 2.3: Frequency of occurrence of cross-correlation values for Gold codes of length $N = 2^n - 1$, n odd [1].

cross-correlation value	frequency of occurrence
-1	$2^{N-1} - 1$
$-[2^{(n+1)/2} + 1]$	$2^{N-2} - 2^{(N-3)/2}$
$2^{(n+1)/2} - 1$	$2^{N-2} + 2^{(N-3)/2}$

There are several ways to generate Walsh sequences, but the easiest way is the use of Hadamard matrices. The orders of Hadamard matrices are restricted to the powers of two, the lowest order Hadamard matrix is defined as

$$H_2 = \begin{bmatrix} 1 & 1 \\ 1 & -1 \end{bmatrix}. \tag{2.9}$$

Higher order matrices are generated with

$$H_K = H_{K/2} \otimes H_2 \tag{2.10}$$

where $\otimes$ denotes Kronecker product. In order to define Kronecker product we need two matrices A and B. Let A be an $n \times n$ matrix with entries a_{ij} and B an $m \times m$ matrix. The Kronecker product of A and B is the $mn \times mn$ block matrix

$$A \otimes B = \begin{bmatrix} a_{11}B & \dots & a_{1n}B \\ \vdots & \ddots & \vdots \\ a_{n1}B & \dots & a_{nn}B \end{bmatrix} \tag{2.11}$$

The Kronecker product is also known as the direct product or the tensor product. So, by means of this method N codes of length N, for $N = 2, 4, 8, 16, 32, ...$ may be generated.

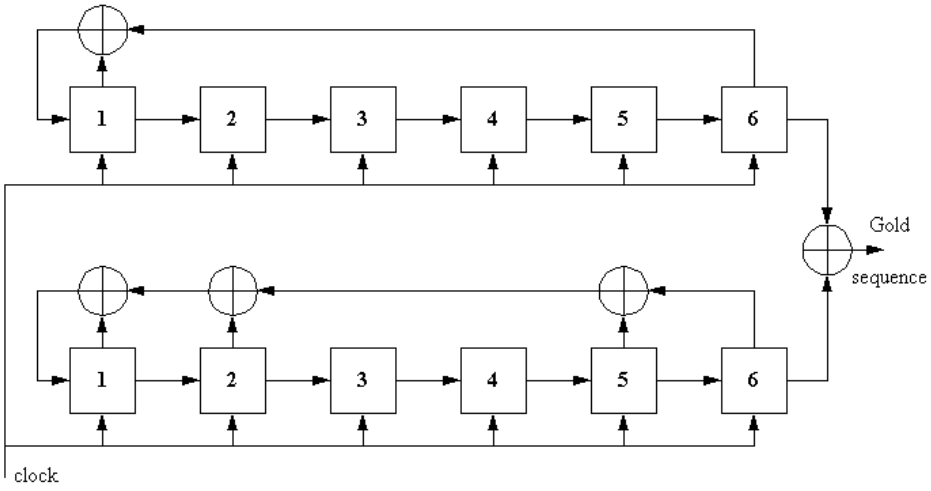

Figure 2.16: A Gold sequence generator of 6-elements [2]

However, the auto-correlation function of Walsh codes does not have good characteristics. It can have more than one peak and therefore, it is not possible for the receiver to detect the beginning of the codeword without an external synchronization scheme. Although the full-sequence cross-correlation is identically zero, this does not hold for partial-sequence cross-correlation function. This is why Walsh codes can only be used in synchronous CDMA. Additionally, Walsh codes do not have the best spreading behavior. They do not spread data as well as m and Gold sequences do because their power spectral density is concentrated in a small number of discrete frequencies.

These drawbacks make Walsh codes not suitable for non-cellular systems. Systems in which Walsh sequences are applied are for instance multi-carrier CDMA and the cellular CDMA system (IS-95). Both systems are based on a cellular concept, all users (and so all interferers) are synchronized with each other. Multi-carrier CDMA uses

another way of spreading while IS-95 uses a combination of a Walsh-sequence and a shift register sequence to enable synchronization.

2.4.3 Synchronous CDMA Model

For a basic synchronous CDMA system, we have the following channel model with K users:

$$r(t) = \sum_{k=1}^{K} A_k \; b_k \; s_k(t) + \sigma \; n(t), \quad t \in [0, T] \tag{2.12}$$

where T is the inverse of data rate, $s_k(t)$ is the signature waveform assigned to the kth user, A_k is the received amplitude of the kth user's signal, $b_k \in \{-1, +1\}$ is the bit transmitted by the kth user, $n(t)$ is the additive white Gaussian noise (AWGN) with unity power spectral density, and finally σ is the standard deviation of the noise.

2.4.4 Asynchronous CDMA Model

Following from Figure 2.17, $\tau \in [0, T)$ is called the offset value. In asynchronous case users send a stream of bits:

$$b_k[-M], \ldots, b_k[0], \ldots, b_k[M]. \tag{2.13}$$

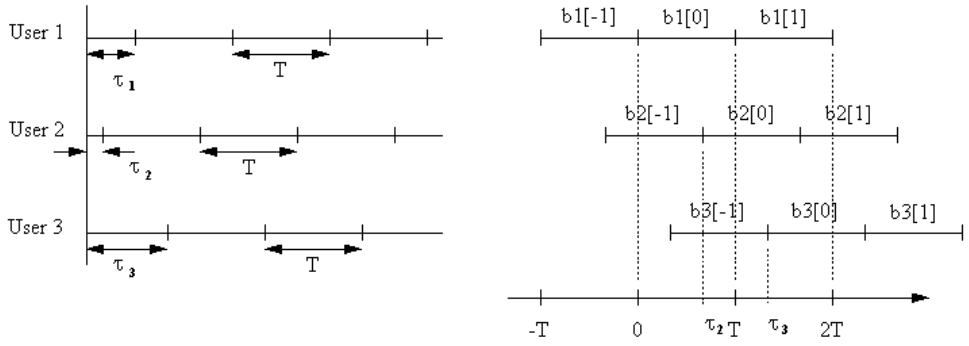

Figure 2.17: Asynchronous CDMA model

We assume here that the length of the frames or packets transmitted by each user is equal to $2M + 1$.

Using these assumption and definitions, the basic asynchronous CDMA channel model becomes:

$$r(t) = \sum_{k=1}^{K} \sum_{i=-M}^{M} A_k \; b_k[i] \; s_k(t - iT - \tau_k) + \sigma \; n(t). \tag{2.14}$$

As already seen in (2.14), the synchronous channel corresponds to a special case of asynchronous channel when all offsets are identical.

2.4.5 Matched Filter

A basic way of converting the received signal into a discrete-time process is to pass it through a bank of matched filters each matched to the signature waveform of a different user and sampling their outputs every T seconds, as shown in Figure 2.18.

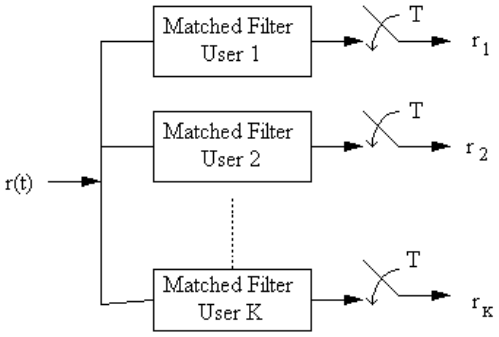

Figure 2.18: Bank of matched filters

In the synchronous case the output of the bank of matched filters are

$$\begin{aligned} r_1 &= \int_0^T r(t)\ s_1(t)\ dt \\ &\vdots \\ r_K &= \int_0^T r(t)\ s_K(t)\ dt \end{aligned} \tag{2.15}$$

The output of the kth matched filter is

$$r_k = A_k\ b_k + \sum_{j \neq k} A_j\ b_j\ \rho_{jk} + n_k \tag{2.16}$$

where

$$\rho_{jk} = \langle s_j, s_k \rangle = \int_0^T s_j(t) s_k(t) dt, \tag{2.17}$$

and

$$n_k = \sigma \int_0^T n(t)\ s_k(t)\ dt. \tag{2.18}$$

In vector form it is

$$\mathbf{r = R\ A\ b + n} \tag{2.19}$$

where $\mathbf{R}$ is the $K \times K$ normalized cross-correlation matrix with (j,k)th element $R_{jk} = \rho_{jk}$,

$$\begin{aligned} \mathbf{r} &= [r_1,\ \ldots,\ r_K]^T, \\ \mathbf{b} &= [b_1,\ \ldots,\ b_K]^T, \\ \mathbf{A} &= \mathrm{diag}[A_1,\ \ldots,\ A_K]^T. \end{aligned}$$

Here diag[$\cdot$] is used to denote a diagonal matrix with entries given in square brackets.

In asynchronous case, for the sake of simplicity, we assume $\tau_1 \leq \tau_2 \leq \ldots \leq \tau_K$, then the matched filter outputs are

$$\begin{aligned} r_k[i] = A_k\ b_k[i] + \sum_{j<k} A_j\ b_j[i+1]\ \rho_{kj} + \sum_{j<k} A_j\ b_j[i]\ \rho_{jk} \\ + \sum_{j>k} A_j\ b_j[i]\ \rho_{kj} + \sum_{j>k} A_j\ b_j[i-1]\ \rho_{jk} + n_k[i] \end{aligned} \tag{2.20}$$

where

$$n_k[i] = \sigma \int_{\tau_k+iT}^{\tau_k+iT+T} n(t)\ s_k(t - iT - \tau_k)\ dt. \tag{2.21}$$

2.4.6 Optimal Receiver for the Single User Channel

If we think of that there is only one user in the channel, the received signal is

$$r(t) = A\ b\ s(t) + \sigma\ n(t). \tag{2.22}$$

Then the decision statistic may be expressed as

$$\hat{b} = \mathrm{sgn}(< r,\ s >) = \mathrm{sgn}\left(\int_0^T r(t)\ s(t)\ dt \right). \tag{2.23}$$

Here and later, the symbol ‘ $\hat{\cdot}$ ’ is used in order to denote an estimate of the variable it is used with and the definition of $\mathrm{sgn}(x)$ is given by

$$\text{sgn}(x) = \begin{cases} -1 & , \quad x < 0 \\ 0 & , \quad x = 0 \\ 1 & , \quad x > 0. \end{cases} \tag{2.24}$$

The probability of error in this case is given as

$$P = Q\left(\frac{A}{\sigma}\right) \tag{2.25}$$

where

$$Q(x) = \int_x^\infty \frac{1}{\sqrt{2\pi}}\, e^{-t^2/2}\, dt. \tag{2.26}$$

CHAPTER 3

DETECTOR TYPES FOR CDMA

After giving the basic definitions for a CDMA system, we may now mention some basic detector types for CDMA, beginning with the single-user matched filter detector.

3.1 Single-User Matched Filter

In most DS-SS systems analysis, the interfering users are assumed to behave like Gaussian noise. Thus, the problem of detecting which signal is transmitted reduces to the detection of the transmitted signal for an AWGN channel in the single-user case. The solution to this problem is known as the maximum likelihood (ML) detector for equally likely transmitted symbols [19]. This corresponds to finding the symbol that was most likely sent given the observed signal as

$$\hat{b} = \arg\max_{b} f(r|b) \tag{3.1}$$

where $\hat{b}$ is the estimated symbol and y is the received signal. If we represent an observed signal in additive white Gaussian noise as

$$r = Ab + n \tag{3.2}$$

where again A is the received amplitude, b is the transmitted bit and n is the AWGN with zero mean and variance, σ^2, then our problem reduces to the hypothesis testing problem of

$$f(r|b=-1) \underset{\hat{b}=1}{\overset{\hat{b}=-1}{\gtrless}} f(r|b=1). \tag{3.3}$$

And substituting the pdfs in (3.3) we get

$$\frac{1}{\sqrt{2\pi}\sigma} e^{\frac{(r+A)^2}{2\sigma^2}} \underset{\hat{b}=1}{\overset{\hat{b}=-1}{\lessgtr}} \frac{1}{\sqrt{2\pi}\sigma} e^{\frac{(r-A)^2}{2\sigma^2}} \tag{3.4}$$

which results in

$$\begin{array}{ccc} & \hat{b} = -1 & \\ Ar & \gtrless & 0. \\ & \hat{b} = 1 & \end{array} \tag{3.5}$$

In this manner, single-user matched filter detector is a type of detector that uses the matched filter bank, we define in section 2.4.5, where each filter is matched to the signature waveform of a different user. The sign of the output of any filter is the estimation of the desired decision, corresponding to transmitted bit $b \in \{+1, -1\}$. This detector is shown in Figure 3.1.

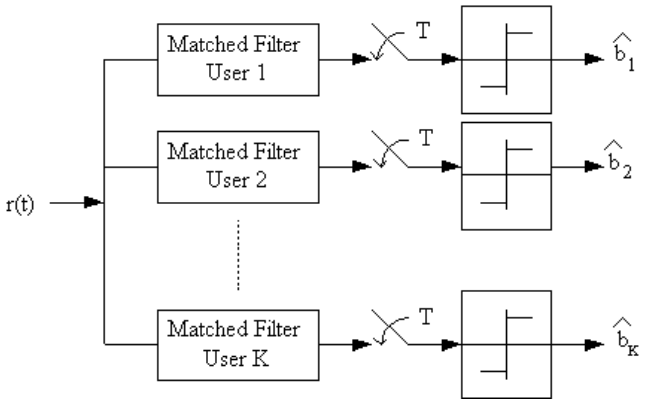

Figure 3.1: Bank of single-user matched filters

The output of the matched filter for the kth user is

$$r_k = \int_0^T r(t)\ s_k(t)\ dt = A_k\ b_k + \sum_{j \neq k} A_j\ b_j\ \rho_{jk} + n_k \tag{3.6}$$

where again

$$n_k = \sigma \int_0^T n(t)\ s_k(t)\ dt, \tag{3.7}$$

then in orthogonal case, the probability of error of user-k is given as

$$P_k(\sigma) = Q\left(\frac{A_k}{\sigma}\right) \tag{3.8}$$

whereas in nonorthogonal case it is

$$P_k(\sigma) = Q\left(\frac{A_k}{\sqrt{\sigma^2 + \sum_{j \neq k} A_j^2 \rho_{jk}^2}}\right), \tag{3.9}$$

and in two-user case for user-1 it is

$$P_1(\sigma) = \frac{1}{2}\, Q\left(\frac{A_1 - A_2\ \rho}{\sigma}\right) + \frac{1}{2}\, Q\left(\frac{A_1 + A_2\ \rho}{\sigma}\right). \tag{3.10}$$

Single-user matched filter detector is also referred to as the conventional receiver.

3.1.1 Asymptotic Multiuser Efficiency

Asymptotic multiuser efficiency is an alternative measure for the multiuser bit-error-rate. It is defined as the ratio between the effective and the actual energies, as

$$\eta_k = \lim_{\sigma\ \to\ 0} \frac{e_k(\sigma)}{A_k^2}. \tag{3.11}$$

Effective energy of user-k, $e_k(\sigma)$, is the energy that user-k would require to achieve the same bit-error-rate of a single user Gaussian channel with the same noise level

$$P_k(\sigma) = Q\left(\frac{\sqrt{e_k(\sigma)}}{\sigma}\right) \geq Q\left(\frac{A_k}{\sigma}\right). \tag{3.12}$$

3.1.2 Near-Far Resistance

Near-far problem is the situation that occurs when the desired user is physically far away from the receiver while any interfering user is closer. Then the interferer is received with greater power and hence, easier to demodulate. If detector is insensitive to the different power levels received, then it is said to be near-far resistant. Near-far resistance is defined related to the multiuser asymptotic efficiency as

$$\bar{\eta_k} = \inf_{A_j>0,\ j\neq k}\ (\eta_k). \tag{3.13}$$

$\inf(\cdot)$ here represents the infimum or the greatest lower bound. In order to define infimum, we use a given set S, if we construct the set L of lower bounds of S, the infimum or the greatest lower bound of set S is the largest member of L.

On condition that the near-far resistance $\bar{\eta} = 0$, the receiver is said to be near-far limited, and if $\bar{\eta} > 0$, the receiver is said to be near-far resistant.

3.2 Optimum Multiuser Detector

Optimum multiuser detector yields the minimum achievable probability of error, optimum multiuser efficiency and near-far resistance.

It is assumed that the receiver not only knows (as in conventional receiver) the signature waveforms and the timing of every active user (for synchronous channels), but it also knows (or can estimate) the received amplitudes of all users and the noise level.

For two-user case, the received signal is

$$r(t) = A_1\ b_1\ s_1(t) + A_2\ b_2\ s_2(t) + \sigma\ n(t). \tag{3.14}$$

Since the bit streams are equiprobable and independent, maximum-likelihood decision rule is used which selects the pair that maximizes

$$f\left[\ \{r(t),\ 0 \le t \le T\ \}|\ (b_1,\ b_2)\ \right] = \exp\left\{-\frac{1}{2\sigma^2}\int_0^T [r(t) - A_1\ b_1\ s_1(t) - A_2\ b_2\ s_2(t)]^2\ dt\right\}. \tag{3.15}$$

$(\hat{b}_1,\ \hat{b}_2)$ is chosen such that $A_1\ \hat{b}_1\ s_1(t) + A_2\ \hat{b}_2\ s_2(t)$ is closest to the received signal in the mean-square sense. For the two-user synchronous channel the likelihood function may be rewritten as

$$f\left[\{r(t), 0 \le t \le T\}|(b_1, b_2)\right] = \exp\left(\frac{1}{\sigma^2}\Omega(b_1,\ b_2)\right)\exp\left(-\frac{A_1^2 + A_2^2}{2\sigma^2}\right)\exp\left(-\frac{1}{2\sigma^2}\int_0^T r^2(t)\ dt\right)$$

where

$$\Omega(b_1,\ b_2) = b_1 A_1 r_1 + b_2 A_2 r_2 - b_1 b_2 A_1 A_2 \rho \tag{3.16}$$

and

$$r_k = \int_0^T r(t) s_k(t) dt. \tag{3.17}$$

Maximum-likelihood decisions are then those estimates that maximizes Ω given by:

$$\min\{A_1|r_1|,\ A_2|r_2|\} \ge A_1 A_2|\rho|. \tag{3.18}$$

When the signatures are not correlated the estimates are found as:

$$\hat{b}_1 = \text{sgn}(r_1) \text{ and } \hat{b_2} = \text{sgn}(r_2) \tag{3.19}$$

otherwise

$$\hat{b}_1 = \text{sgn}\left(A_1\ r_1 - \text{sgn}(\rho)\ A_2\ r_2\right) \tag{3.20}$$

$$\hat{b}_2 = \text{sgn}\left(A_2\ r_2 - \text{sgn}(\rho)\ A_1\ r_1\right) \tag{3.21}$$

A K-user, M-frame asynchronous channel may be thought as a $K(2M+1)$-user synchronous channel. Defining a $K(2M+1)$-vector $\mathbf{b}$, with components

$$b_{k+iK} = b_k[i], \quad k = 1,\ 2, \ldots,\ K, \quad i = -M, \ldots,\ M \tag{3.22}$$

the objective here, is to compute $\mathbf{b}$ that maximizes

$$f\left[\ \{\ r(t), t \in [-MT,\ MT+2T]\ \}\ |\ \mathbf{b}\ \right] = \exp\left(-\frac{1}{2\sigma^2}\int_{-MT}^{MT+2T}\left(\ r(t) - S_t(\mathbf{b})\ \right)^2 dt\right) \tag{3.23}$$

where

$$S_t(\mathbf{b}) = \sum_{k=1}^{K}\sum_{i=-M}^{M} A_k\ b_k[i]\ s_k(t - iT - \tau_k) \tag{3.24}$$

An illustration of a two-user asynchronous channel frames is given in Figure 3.2 and in Figure 3.3, a block diagram of an optimum detector for an asynchronous channel is

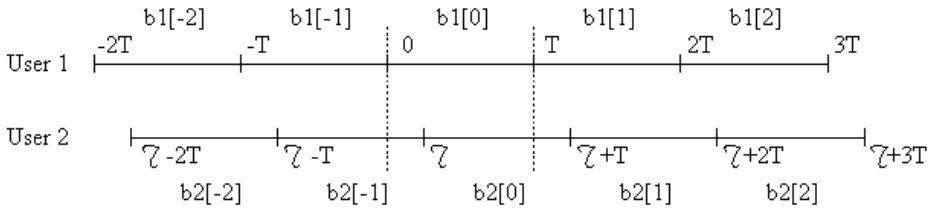

Figure 3.2: Two-user asynchronous case

shown. This detector estimates the transmitted bits maximizing (3.23) by using Viterbi algorithm.

3.3 Decorrelating Detector

The decorrelating detector is derived with the following idea: In the absence of noise, equation (2.19) turns

$$\mathbf{r} = \mathbf{R}\ \mathbf{A}\ \mathbf{b} \tag{3.25}$$

multiplying both sides of above equation by the inverse of $\mathbf{R}$ we get

$$\mathbf{R}^{-1}\ \mathbf{r}\ =\ \mathbf{R}^{-1}\ \mathbf{R}\ \mathbf{A}\ \mathbf{b}\ =\ \ \mathbf{A}\ \mathbf{b} \tag{3.26}$$

where $\mathbf{R}$ is supposed to be invertible. Then the transmitted data is recovered by

$$\hat{b}_k = \operatorname{sgn}\left((\mathbf{R}^{-1}\ \mathbf{r})_k\right) = \operatorname{sgn}\left((\mathbf{A}\ \mathbf{b})_k\right) = b_k. \tag{3.27}$$

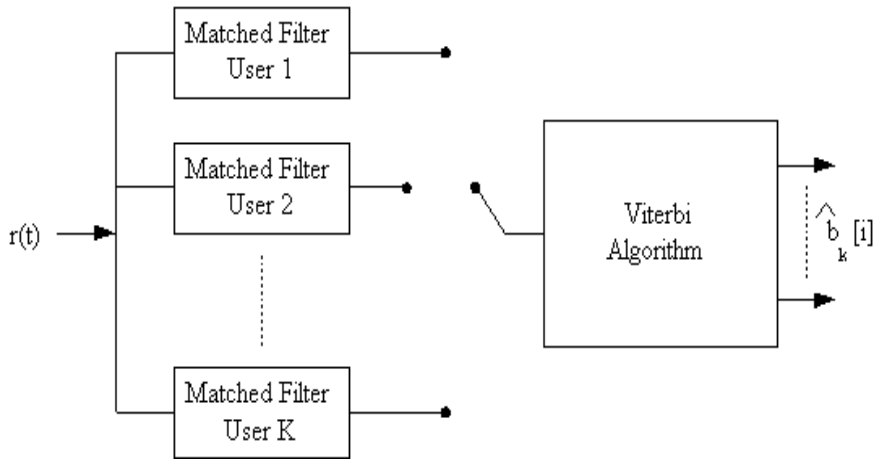

Figure 3.3: Optimum detector for asynchronous channel

If we bring in the noise then (3.26) turns into

$$\mathbf{R}^{-1}\ \mathbf{r}\ =\ \ \mathbf{A}\ \mathbf{b}\ +\ \mathbf{R}^{-1}\ \mathbf{n}. \tag{3.28}$$

The kth component here is free from the interference from other users, that is why this detector is called "decorrelating detector". As it is seen through those derivations, the decorrelating detector disregards the background noise while eliminating the multiple access interference (MAI). The block diagram corresponding to the derived detector is given in Figure 3.4.

Two desirable features of decorrelating detector are that it does not require the knowledge of the received amplitudes and it can be decentralized so that the demodulation of each user can be implemented independently as

$$(\mathbf{R}^{-1}\ \mathbf{r})_k \ = \ \sum_{j=1}^{K} R^{+}_{kj}\ r_j = \sum_{j=1}^{K} R^{+}_{kj}\langle r,\ s_j\rangle = \left\langle r,\ \sum_{j=1}^{K} R^{+}_{kj}\ s_j \right\rangle = \langle r,\ \tilde{s}_k\rangle \tag{3.29}$$

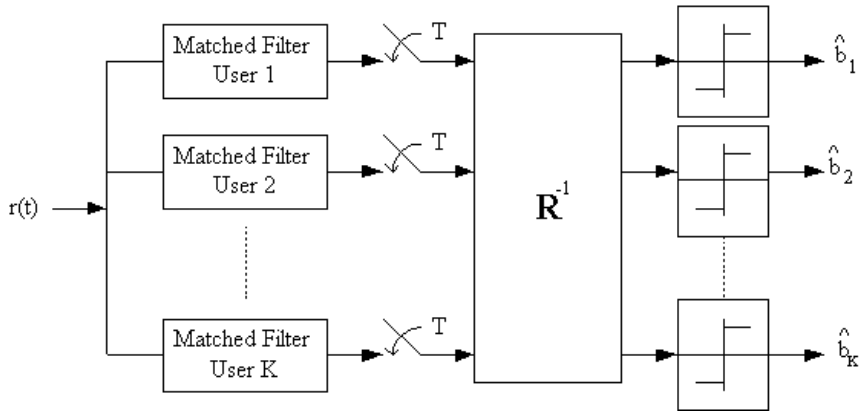

Figure 3.4: Decorrelating detector

where R^{+}_{kj} is a shorthand for $(\mathbf{R}^{-1})_{kj}$ and $\langle x, y\rangle$ defines the inner product of $x(t)$ and $r(t)$ as it is defined in (2.23). With this decentralizable representation the decorrelating detector can be realized as in Figure 3.5.

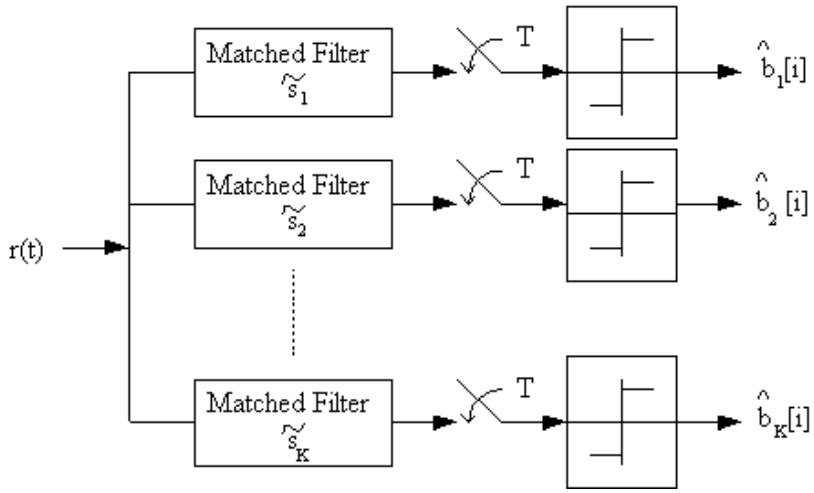

Figure 3.5: Modified decorrelating detector

3.4 MMSE Detector

This detector is derived to minimize the mean-square-error by the following way:

The problem of estimating a random variable W on the basis of observations Z is to chose the function $\hat{W}(Z)$ that minimizes the MSE,

$$\mathrm{E}\left[\left(W - \hat{W}(Z)\right)^2\right]. \tag{3.30}$$

$\mathrm{E}(\cdot)$ is used here to denote the expectation or the statistical averaging operation. The expected or the mean value of a single continuous random variable X is defined as

$$\mathrm{E}(X) = \int_{-\infty}^{\infty} xp(x)dx \tag{3.31}$$

where x denotes the realizations that the random variable X may achieve and $p(x)$ is called the probability density function (PDF) of random variable X.

The solution is the conditional-mean estimator [19]:

$$\hat{W}(Z) = \mathrm{E}(W \mid Z). \tag{3.32}$$

The MMSE linear detector for the kth user chooses the waveform c_k of duration T that achieves

$$\min_{c_k} \mathrm{E}\left[(b_k - \langle c_k,\ r\rangle)^2\right] \tag{3.33}$$

that is, the waveform c_k to be chosen is the one that minimizes the $\mathrm{E}(\cdot)$ operation in 3.33. Then the linear MMSE detector outputs the decision

$$\hat{b}_k = \mathrm{sgn}\left(\langle c_k,\ r\rangle\right). \tag{3.34}$$

Final decision for MMSE linear detector is derived as [16]

$$\hat{b}_k = \mathrm{sgn}\left(\left(\left[\mathbf{R} + \sigma^2\mathbf{A}^{-2}\right]^{-1}\mathbf{r}\right)_k\right). \tag{3.35}$$

The MMSE detector takes both MAI and background noise into account. It is a compromise solution of the conventional receiver and the decorrelating detector, since they are the limiting cases of the MMSE detector. Because following from (3.35), when noise level is very low, the transformation approaches the decorrelating receiver, and when noise is dominant, it becomes like the single-user matched filter. Again from 3.35 it is clear that linear MMSE detector would require received SNRs of users in the system

and also the signature codes in order to build **R**.

The adaptive type MMSE detector requiring no prior knowledge of received SNRs or interfering signature codes will be mentioned later.

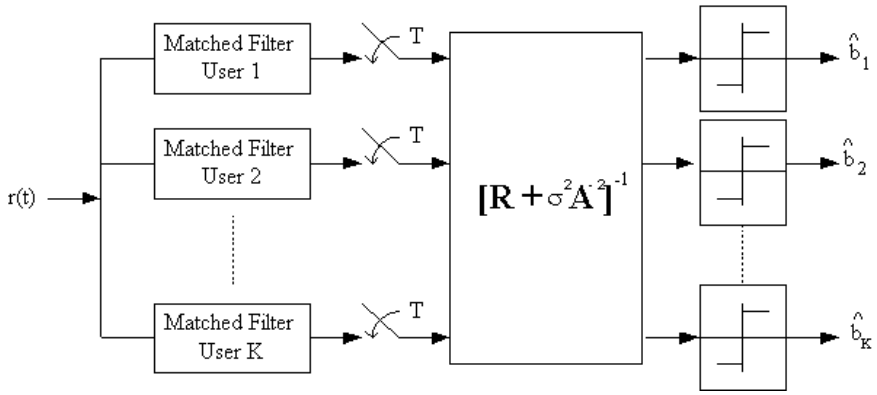

Figure 3.6: MMSE linear detector

3.5 Successive Cancellation

Successive cancellation is built on the simple idea named successive decoding, given in Figure 3.7. This idea is, if a decision is made about an interfering user's bit, then subtracting this interfering signal from the received waveform at the receiver, the effect of this interfering signal is cancelled. Of course, this will be useful when the decision about the interfering signal is correct, otherwise subtracting step will double the effect of the interfering signal.

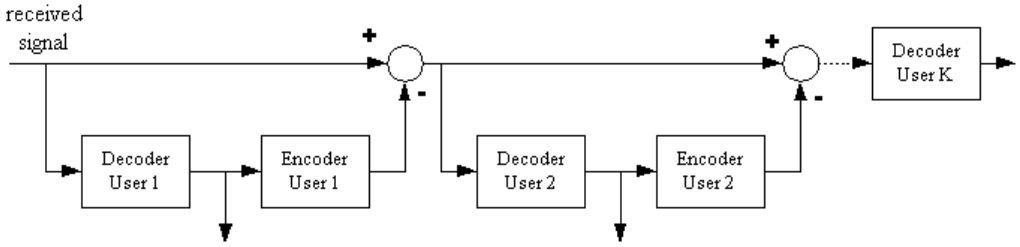

Figure 3.7: Successive Decoding

In simplest form, the successive receiver uses the output of the single-user matched filters, which does not care about the other users' interference. There are several ways of choosing the order of users. One is to demodulate users in order of their decreasing received powers, but this approach is not the best method, since it does not take the cross-correlations among users into account. A sensitive method is to order users according to the average received power at the output of each matched filter given by

$$E\left[\left(\int_0^T r(t)\ s_k(t)\ dt\right)^2\right] = \sigma^2 + A_k^2 + \sum_{j\neq k} A_j^2\ \rho_{jk}^2. \tag{3.36}$$

If we consider the synchronous two-user case, the output of the matched filter detector for User-2 will be

$$\hat{b}_2 = \text{sgn}(r_2) \tag{3.37}$$

Recreating the signal of User-2 with this estimated $\hat{b}_2$, we get $A_2\hat{b}_2 s_2(t)$, then subtracting this from the received signal yields

$$\begin{aligned} \hat{r}(t) &= r(t) - A_2\hat{b}_2 s_2(t) \\ &= A_1 b_1 s_1(t) + A_2(b_2 - \hat{b}_2)s_2(t) + n(t) \end{aligned} \tag{3.38}$$

Then passing $\hat{y}$ through the matched filter for User-1, we reach the following decision

$$\begin{aligned} \hat{b}_1 &= \text{sgn}(\langle \hat{r}\ s_1 \rangle) \\ &= \text{sgn}(r_1 - A_2\hat{b}_2\rho) \\ &= \text{sgn}(r_1 - A_2\ \rho\ \text{sgn}(r_2)) \\ &= \text{sgn}(A_1 b_1 + A_2(b_2 - \hat{b}_2)\rho + \sigma\langle n,\ s_1\rangle) \end{aligned} \tag{3.39}$$

3.6 Adaptive MMSE Detector

In section 3.4 it is mentioned that MMSE detector minimizes the squared error between the transmitted bit and the filter output. If user-1 is the desired user, the cost function given by (3.33) becomes

$$\text{E}\left[(b_1 - \langle c_1,\ r\rangle)^2\right] \tag{3.40}$$

where b_1 is the actual transmitted bit. In each frame of symbols one bit which is known at the receiver is sent resulting in a training sequence of known chips at the receiver. Using this already known data bit, it is shown in [16] that MMSE detector c_k may be computed adaptively. For this an iterative algorithm named as gradient descent is preferred. According to this algorithm, the computed MMSE detector c_k is given as

$$c_k[n] = c_k[n-1] - \mu(c_k^T[n-1]r[n] - b_k[n])r[n] \tag{3.41}$$

where μ represents the step size. It is shown in [16] that this equation is globally convergent when μ decreases suitably. In order to provide that, μ is suggested to be $\mu(n) = 1/(n+p)$ where p is a design parameter. At the beginning n will be small. Hence, $\mu(n)$ will be large and thus the convergence rate will be high. As c_k converges to actual c_k, accuracy will be more important and a small μ will be needed.

In order to compute the detector iteratively, adaptive MMSE detector just requires the training sequence and the timing of the user. No signature code, including the desired user, is required.

3.7 Minimum Output Energy Detector

The mean output energy (MOE) is defined as

$$\mathrm{E}\left[(\langle r, c_k\rangle)^2\right] \tag{3.42}$$

This detector estimates the detector c_k that minimizes this mean output energy. This term in (3.42) is also equal to the variance of the filter output at time T. Therefore, this detector is also called as minimum variance detector. The MOE given by (3.42) and the MSE given by (3.33) have the following relation

$$\begin{aligned}
\mathrm{MSE}(x_1) &= \mathrm{E}\left[(A_1 b_1 - \langle r, s_1 + x_1\rangle)^2\right] \\
&= \mathrm{E}\left[(A_1^2 b_1^2 - 2A_1 b_1 \langle r, s_1 + x_1\rangle) + (\langle r, s_1 + x_1\rangle)^2\right] \\
&= A_1^2 - 2A_1 \mathrm{E}\left[b_1 \langle r, s_1 + x_1\rangle\right] + \mathrm{MOE}(x_1) \\
&= A_1^2 - 2A_1^2 \langle s_1, s_1 + x_1\rangle + \mathrm{MOE}(x_1) \\
\mathrm{MSE}(x_1) &= \mathrm{MOE}(x_1) - A_1^2
\end{aligned} \tag{3.43}$$

This shows that minimizing MOE is equivalent to minimizing MSE. The filter coefficients that are found by minimizing MOE will also minimize MSE. Furthermore, since the cost function of MOE does not contain b_1, blind adaptive algorithms are applicable in this situation.

3.8 Performance Comparison of CDMA Detectors

In this section the performances of the accounted detectors are compared based on simulation studies. Figure 3.8 shows the asymptotic efficiency performance of different CDMA schemes. Two users were assumed. User-1 is chosen as the user of interest and it has fixed power of $\mathrm{SNR}_1 = 25$ dB whereas the second users received power is varied to plot the asymptotic efficiency with respect to users' received amplitude ratios. The simulation results match well with the results obtained in [16].

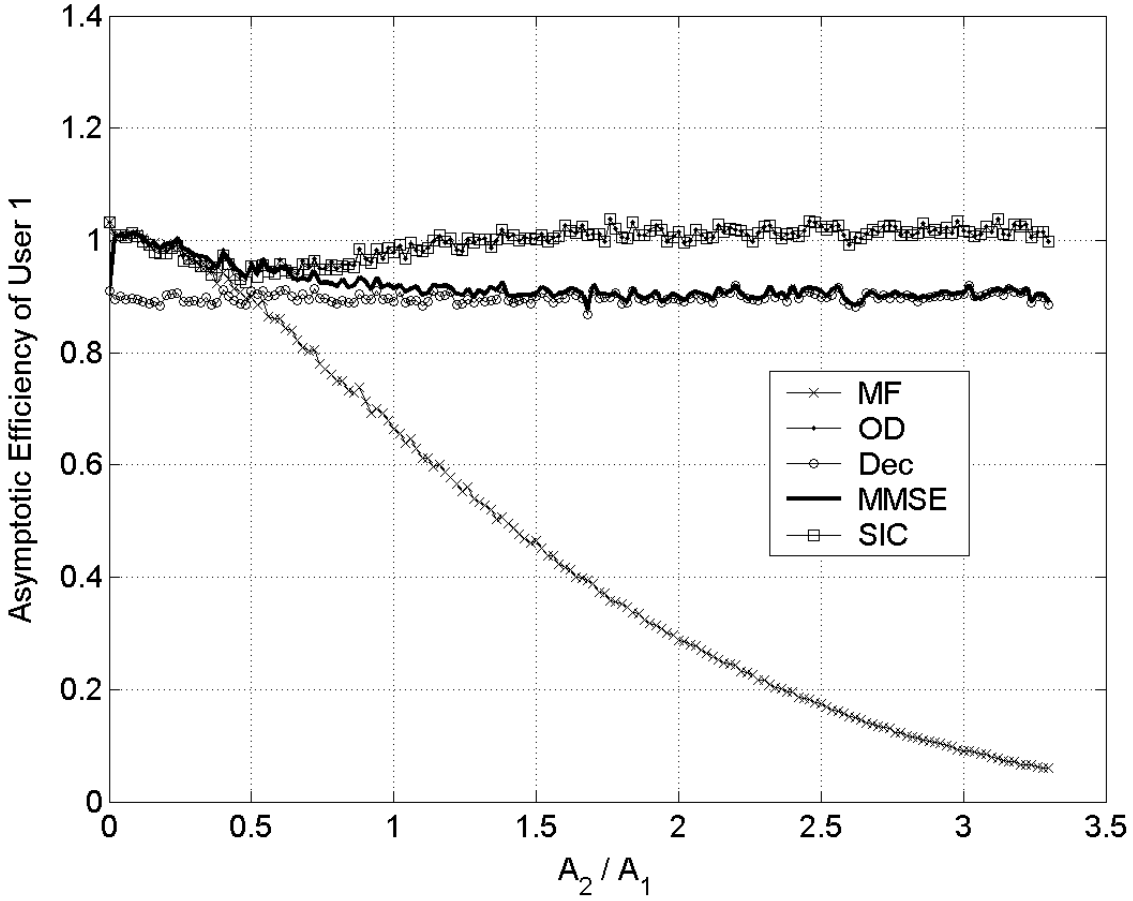

Figure 3.8: Comparison of asymptotic multiuser efficiencies

The optimum detector performs the best and is closely approximated by the SIC scheme. These detectors achieve nearly the ultimate performance of unity asymptotic efficiency and their superiority to other detectors becomes obvious when the SIR decreases below unity. The MMSE detector is the optimum linear detector, it takes both MAI and the additive noise into account and thus it shows close to optimum performance for higher SIR values, but as the SIR ratio decreases its asymptotic efficiency converges to the one of the decorrelating receiver. because the effect of the additive noise becomes negligible for high MAI. The asymptotic efficiency of user-1 is approximately 0.9 fo high values

of MAI when either MMSE or decorrelating detectors are used. On the other hand the single-user detector (SUD) performs very badly and when SUD is used the asymptotic efficiency of user-1 tends to zero as the MAI increases as expected.

Figure 3.9 plots the BER performance of the schemes with respect to increasing number of users with equal received powers. The SNR for each user is 10 dB. The optimum detector performs significantly better than the rest, but this result is obtained with a price of increased complexity.

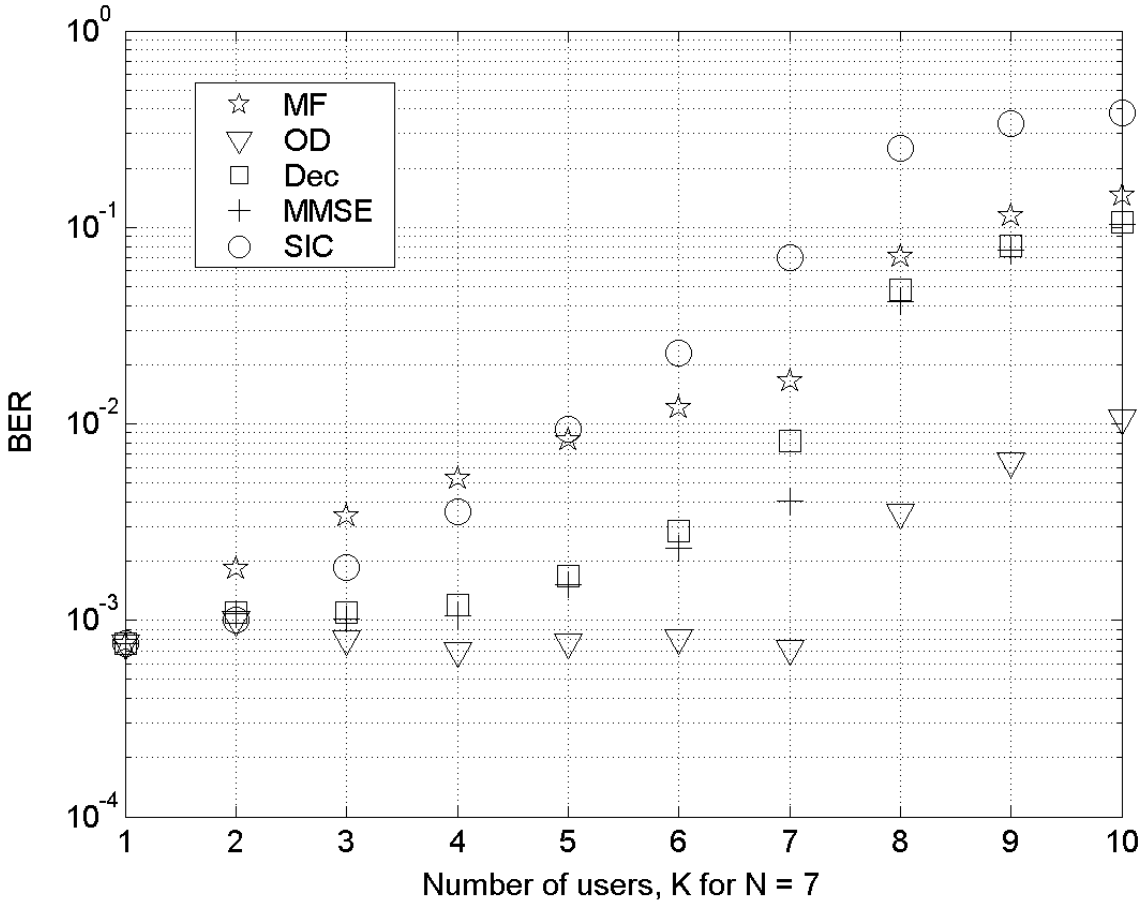

Figure 3.9: Comparison of BERs wrt number of users

We should note here that the SIC detector does not perform well in the presence of many users with equal received powers. Its performance is even worse than the performance of the SUD for number of users higher than four. Also, as the number of users increases the interference becomes much more effective than the additive noise. Thus, the MMSE and decorrelator detectors converge to the same level as the number of users increases.

CHAPTER 4

BLIND MULTIUSER DETECTION

The word *blind* stands for that the receiver does not have any prior knowledge about the received signal except the signature waveform of the desired user. Thus, blind detectors are useful especially for downlinks of CDMA systems in practice, because, it provides for the ability of a mobile terminal to communicate with just using its own signature waveform. So, neither obtaining any information about other users such as their signature waveforms nor any training sequence is necessary for blind multiuser detection. Additionally, not using any training sequence in downlink will result in economical use of channel bandwidth. On the other hand, for uplink detection, the receiver, say base station, does not necessarily use blind techniques since it already has the knowledge of all signature waveforms of users within a cell. And also, for a base station any physical enlargement for a better performing detection scheme is not as much a problem as it is for a mobile unit.

In this chapter, we will pay attention especially on the adaptive blind MMSE detectors derived using subspace approach [6], and the reduced-rank approach [8]. Before we derive our blind adaptive MMSE detector, we should make some definitions and assumptions for our signal model.

4.1 Signal Model

A DS-CDMA system with K users that are simultaneously communicating through an AWGN channel, is considered. The received baseband signal at the receiver can be modelled as

$$r(t) = \sum_{k=1}^{K} A_k \sum_{i=-\infty}^{\infty} b_k(i)\ s_k(t - iT - \tau_k) + \sigma n(t). \tag{4.1}$$

As described before, A_k, here is the received amplitude of user-k. $b_k(i)$ is the information bit of user-k in the ith bit interval. $s_k(t)$ is the normalized signature waveform of user-k as defined in (4.2). τ_k is propagation delay with respect to the receiver, and $n(t)$ is zero-mean AWGN with power spectral density σ^2.

$$s_k(t) = \frac{1}{\sqrt{N}} \sum_{j=0}^{N-1} s_k[j]\ \psi(t - j\ T_c), \quad t \in [0,\ T] \tag{4.2}$$

where $\{s_k[0],\ s_k[1], \ldots,\ s_k[N-1]\}$ is the signature sequence of user-k, $\psi(t)$ is a normalized chip waveform of duration T_c. If all users are transmitting synchronously, then $\tau_1 = \tau_2 = \ldots = \tau_K = 0$, and the received signal may be considered during one bit interval, resulting in the representation

$$r(t) = \sum_{k=1}^{K} A_k\ b_k\ s_k(t) + \sigma n(t), \quad t \in [0,\ T]. \tag{4.3}$$

Passing the signal in (4.3) through a matched filter, matched to chip waveform $\psi(T-t)$ and sampling at chip rate, during one bit interval we obtain an N-vector like

$$\mathbf{r} = \sum_{k=1}^{K} A_k\ b_k\ \mathbf{s}_k + \sigma \mathbf{n}, \tag{4.4}$$

where $\mathbf{s}_k = (1/\sqrt{N})\ [\ s_k[0],\ s_k[1], \ldots,\ s_k[N-1]\ ]^T$ is the normalized signature waveform of user-k, and $\mathbf{n}$ is a WGN vector with zero-mean and covariance matrix $\sigma^2\ \mathbf{I}_N$. The equation (4.4) may be rewritten as

$$\mathbf{r} = \mathbf{S}\ \mathbf{A}\ \mathbf{b}\ + \sigma \mathbf{n}, \tag{4.5}$$

where $\mathbf{S} = [\mathbf{s}_1,\ \mathbf{s}_2, \ldots,\ \mathbf{s}_K]$, $\mathbf{A} = \mathrm{diag}(A_1,\ A_2, \ldots,\ A_K)$, and $\mathbf{b} = [b_1,\ b_2, \ldots,\ b_K]^T$.

4.2 Classical Blind Source Separation

The classical blind source separation (BSS) schemes are based on the assumption of independent components in the received signal streams. This is valid if the data carried in the received signal is random. Independent component analysis (ICA) and its variations like fastICA that solves the problem by extracting the independent components step by step, and some batch type algorithms like joint approximate diagonalization of eigen-matrices (JADE) [20] and blind source separation algorithm with reference system (SSARS) [21] are in this class of BSS techniques.

Although this thesis mostly concentrates on subspace approach, for comparison

one such algorithm, JADE will be mentioned next, as an example for batch type BSS.

4.2.1 JADE

JADE algorithm is a batch algorithm for solving the separation problem. The first step of JADE is to decorrelate received streams in $\mathbf{r}$. For this a $K \times N$ matrix $\mathbf{W}$, named whitening matrix, is calculated that satisfies

$$\mathbf{I} = \mathbf{W}\mathbf{C}\mathbf{W}^T \tag{4.6}$$

where $\mathbf{C} = \mathrm{E}\left\{\mathbf{r}\ \mathbf{r}^T\right\}$ is the auto-correlation matrix of the received signals. In BSS this step is called principle component analysis and can be solved using an eigenvalue decomposition of $\mathbf{C}$. The decorrelation is done by

$$\mathbf{z} = \mathbf{W}\ \mathbf{r}. \tag{4.7}$$

JADE uses fourth-order statistics. It maximizes some elements of the cumulant matrix $\mathbf{Q_z} = \mathrm{cum}(b_i, b_j, b_k, b_l),\ i, j, k, l \leq K$ obtained from the extracted signals $\mathbf{b}$ in (4.9). The optimization problem is solved by an eigenvalue decomposition of $\mathbf{Q_z}$ and a joint diagonalization of the dominant eigenvectors rearranged as matrices. This diagonalization leads to the unitary matrix $\mathbf{B}$

$$\max_{\mathbf{B}} = \sum_{i,j,k,l=1}^{K} |\mathrm{cum}(b_i, b_j, b_k, b_l)|^2 \tag{4.8}$$

and the independent data streams are

$$\mathbf{b} = \mathbf{B}^T\mathbf{z}. \tag{4.9}$$

The JADE algorithm can be summarized by the following steps [20]:

- Step-1: Form the sample covariance matrix $\hat{\mathbf{C}}$ and compute a whitening matrix $\hat{\mathbf{W}}$.
- Step-2: Form the sample fourth-order cumulants $\hat{\mathbf{Q}}_z$ of the whitened process $\hat{\mathbf{z}} = \hat{\mathbf{W}}\hat{\mathbf{r}}$; compute the K most significant eigen-pairs $\{\hat{\lambda}_k, \hat{\mathbf{u}}_k | 1 \leq k \leq K\}$.
- Step-3: Jointly diagonalize the set $\{\hat{\lambda}_k\hat{\mathbf{u}}_k | 1 \leq k \leq K\}$ by a unitary matrix $\hat{\mathbf{B}}$.
- Step-4: Estimate b as $\hat{b} = \hat{\mathbf{B}}^T\hat{\mathbf{z}}$.

4.3 Subspace Concept

The autocorrelation matrix of the received signal $\mathbf{r}$ is given by

$$\mathbf{C} = \mathrm{E}\{\mathbf{r}\mathbf{r}^T\} = \sum_{k=1}^{K} A_k^2 \ \mathbf{s}_k \ \mathbf{s}_k^T + \sigma^2 \ \mathbf{I}_N = \mathbf{S} \ \mathbf{A}^2 \ \mathbf{S}^T + \sigma^2 \ \mathbf{I}_N. \tag{4.10}$$

Performing an eigen-decomposition, the autocorrelation matrix $\mathbf{C}$ may also be expressed as

$$\mathbf{C} = \mathbf{U}\mathbf{\Lambda}\mathbf{U}^T = [\mathbf{U}_s \ \mathbf{U}_n] \begin{bmatrix} \mathbf{\Lambda}_s & \\ & \mathbf{\Lambda}_n \end{bmatrix} \begin{bmatrix} \mathbf{U}_s^T \\ \mathbf{U}_n^T \end{bmatrix} \tag{4.11}$$

where $\mathbf{U} = [\mathbf{U}_s \ \mathbf{U}_n]$, $\mathbf{\Lambda} = \mathrm{diag}\,(\mathbf{\Lambda}_s \ \mathbf{\Lambda}_n)$, $\mathbf{\Lambda}_s = \mathrm{diag}\,(\lambda_1, \ \ldots, \ \lambda_K)$ contains the K largest eigenvalues of $\mathbf{C}$ in descending order, and $\mathbf{U}_s = [\mathbf{u}_1 \ \ldots \ \mathbf{u}_K]$ contains the corresponding orthonormal eigenvectors, $\mathbf{\Lambda}_n = \sigma^2\mathbf{I}_{N-K}$ and $\mathbf{U}_n = [\mathbf{u}_{K+1} \ \ldots \ \mathbf{u}_N]$ contains the $N-K$ orthonormal eigenvectors corresponding to the eigenvalue σ^2. The range space of $\mathbf{U}_s$ is called signal subspace since it has the range as $\mathbf{S}$. The range of $\mathbf{U}_n$ is called the noise subspace. Defining an $N \times N$ diagonal matrix as

$$\mathbf{\Lambda}_0 \stackrel{\Delta}{=} \mathbf{\Lambda} - \sigma^2\mathbf{I}_N = \mathrm{diag}(\lambda_1 - \sigma^2, \ \ldots \ , \lambda_K - \sigma^2, \ 0, \ \ldots \ , \ 0), \tag{4.12}$$

and by using equations (4.10), and (4.11) we obtain

$$\mathbf{S} \ \mathbf{A}^2\mathbf{S}^T = \mathbf{U}_s(\mathbf{\Lambda}_s - \sigma^2\mathbf{I}_K)\mathbf{U}_s^T = \mathbf{U}\mathbf{\Lambda}_0\mathbf{U}^T. \tag{4.13}$$

Deciding the k^{th} user data bit, we define a linear multiuser detector in the following form

$$\hat{b}_k = \mathrm{sgn}(\boldsymbol{\omega}_k^T\mathbf{r}) \tag{4.14}$$

where $\boldsymbol{\omega}_k \in \mathcal{R}^N$. Next the linear MMSE detector will be derived in terms of signal subspace parameters $\{\mathbf{U}_s, \ \mathbf{\Lambda}_s$, and $\sigma\}$.

4.3.1 Formulation of the Linear MMSE Detector with the Subspace Concept

Assuming that the desired user is user-1, let's denote the filter coefficients for user-1 with the weight vector $\boldsymbol{\omega}_1 = \mathbf{m}_1$ where $\mathbf{m}_1 \in \mathcal{R}^N$. The vector $\mathbf{m}_1$ is chosen as such a vector that minimizes the MSE and it is defined as

$$\mathrm{MSE}(\mathbf{m}_1) \triangleq \mathrm{E}\{(A_1 b_1 - \mathbf{m}_1^T \mathbf{r}^2)\} \tag{4.15}$$

subject to $\mathbf{m}_1^T \mathbf{s}_1 = 1$.

Using signal subspace parameters, the linear MMSE detector $\mathbf{m}_1$ is given by

$$\mathbf{m}_1 = \frac{\mathbf{U}_s \mathbf{\Lambda}_s^{-1} \mathbf{U}_s^T \mathbf{s}_1}{\mathbf{s}_1^T \mathbf{U}_s \mathbf{\Lambda}_s^{-1} \mathbf{U}_s^T \mathbf{s}_1} \tag{4.16}$$

Proof [6]: Using (4.4) and (4.15), by the method of Lagrange multipliers, we obtain

$$\begin{aligned}
\mathcal{L}(\mathbf{m}) &\triangleq \mathrm{MSE}(\mathbf{m}) - 2\mu(\mathbf{m}^T \mathbf{s}_1 - 1) \\
&= \mathbf{m}^T \underbrace{\mathrm{E}\{\mathbf{r}\mathbf{r}^T\}}_{\mathbf{C}} \mathbf{m} - 2A_1 \mathbf{m}^T \underbrace{\mathrm{E}\{b_1 \mathbf{r}\}}_{\mathbf{s}_1} + A_1^2 - 2\mu(\mathbf{m}^T \mathbf{s}_1 - 1) \\
&= \mathbf{m}^T \mathbf{C}\ \mathbf{m} - 2A_1 \mathbf{m}^T \mathbf{s}_1 + A_1^2 - 2\mu(\mathbf{m}^T \mathbf{s}_1 - 1) \\
&= \mathbf{m}^T \mathbf{C}\ \mathbf{m} - 2(A_1^2 + \mu)\mathbf{m}^T \mathbf{s}_1 + (A_1^2 + 2\mu).
\end{aligned} \tag{4.17}$$

The linear MMSE detector is obtained by solving for $\mathbf{m}_1$ from $\nabla\mathcal{L}(\mathbf{m}_1) = 0$.

$$\begin{aligned}
\nabla\mathcal{L}(\mathbf{m}_1) = 2\mathbf{C}\ \mathbf{m}_1 - 2A_1^2 \mathbf{s}_1 - 2\mu\mathbf{s}_1 &= 0 \\
\mathbf{C}\ \mathbf{m}_1 &= A_1^2 \mathbf{s}_1 + \mu\mathbf{s}_1 \\
\mathbf{m}_1 &= (A_1^2 + \mu)\mathbf{C}^{-1}\mathbf{s}_1 \\
\mathbf{m}_1 &= (A_1^2 + \mu)(\mathbf{U}_s \mathbf{\Lambda}_s^{-1} \mathbf{U}_s^T)\mathbf{s}_1 + (A_1^2 + \mu)\sigma^{-2}(\mathbf{U}_n \mathbf{U}_n^T)\mathbf{s}_1 \\
\mathbf{m}_1 &= (A_1^2 + \mu)(\mathbf{U}_s \mathbf{\Lambda}_s^{-1} \mathbf{U}_s^T)\mathbf{s}_1
\end{aligned} \tag{4.18}$$

where we used the eigen-decomposition of $\mathbf{C}$ given in (4.11), and the last equality follows from the fact that $\mathbf{s}_1 \in \mathrm{range}(\mathbf{U}_s)$ is orthogonal to the noise subspace, i.e, $\mathbf{U}_n^T \mathbf{s}_1 = 0$. And finally, using the constraint that $\mathbf{m}_1^T \mathbf{s}_1 = 1$, we obtain

$$(A_1^2 + \mu) = 1/[\mathbf{s}_1^T \mathbf{U}_s \mathbf{\Lambda}_s^{-1} \mathbf{U}_s^T \mathbf{s}_1]. \tag{4.19}$$

Substituting (4.19) in (4.18) we obtain (4.16).

Since the decision rule (4.14) is invariant to positive scaling on linear MMSE

detector, we use the scaled version of the linear detector $\mathbf{m}_1$ for simplicity, given by

$$\mathbf{m}_1 \triangleq \mathbf{U}_s \mathbf{\Lambda}_s^{-1} \mathbf{U}_s^T \mathbf{s}_1. \tag{4.20}$$

Then, MSE can be found as

$$\text{MSE} = 1 - \mathbf{s}_1^T \mathbf{U}_s \mathbf{\Lambda}_s^{-1} \mathbf{U}_s^T \mathbf{s}_1. \tag{4.21}$$

4.3.2 Subspace Tracking

In the previous sections, we have mentioned the subspace concept. For our blind receivers, the eigen-components of the auto-correlation function $\mathbf{C}$, have to be estimated. Then, tracking the subspace we may build our blind rank-K detector. Two classical approaches to subspace estimation are the batch eigenvalue decomposition (ED) of the sample auto-correlation matrix, or the batch singular value decomposition (SVD) of the data matrix. Disadvantage of those is that they are computationally too expensive for adaptive applications. We need to use such algorithms that are naturally recursive and updating subspace sample-by-sample, like modern subspace tracking algorithms are. As in [6], for our blind adaptive rank-K detector, among several algorithms, we use the adopt version of projection approximation subspace tracking (PASTd) algorithm recently proposed in [22] with the extended version in [5]. Its good convergence to the signal eigenvalues and eigenvectors, low computational complexity of *O(NK)*, and the rank tracking capability are the advantages of this algorithm. Now, let's see how PASTd works for tracking the signal subspace.

Let $\mathbf{r} \in \mathcal{R}^N$ be a random vector with auto-correlation matrix $\mathbf{C} = \text{E}\{\mathbf{r}\mathbf{r}^T\}$. Consider the scalar function

$$J(\mathbf{W}) = \text{E}\{\|\mathbf{r} - \mathbf{W}\mathbf{W}^T\mathbf{r}\|^2\} = \text{tr}(\mathbf{C} - 2\text{tr}(\mathbf{W}^T\mathbf{C}\ \mathbf{W}) + \text{tr}(\mathbf{W}^T\mathbf{C}\ \mathbf{W}\ \mathbf{W}^T\mathbf{W})) \tag{4.22}$$

with a matrix argument $\mathbf{W} \in \mathcal{R}^{N \times r}$ $(r < N)$. It is proved in [22] that

- $\mathbf{W}$ is a stationary point of $J(\mathbf{W})$ if and only if $\mathbf{W} = \mathbf{U}_r\mathbf{Q}$, where $\mathbf{U}_r \in \mathcal{R}^{N \times r}$ contains any r distinct eigenvectors of $\mathbf{C}$ and $\mathbf{Q} \in \mathcal{R}^{r \times r}$ is any unitary matrix.
- All stationary points of $J(\mathbf{W})$ are saddle points except when $\mathbf{U}_r$ contains the r dominant eigenvectors of $\mathbf{C}$. In that case, $J(\mathbf{W})$ attains the global minimum.

So, for $r = 1$, the solution of minimizing $J(\mathbf{W})$ is given by the most dominant eigenvector of $\mathbf{C}$. Since in practice, only the sample vectors $\mathbf{r}(i)$ are available, we may rewrite (4.22) with the exponentially weighted sums as

$$J[\mathbf{W}(t)] = \sum_{i=1}^{t} \beta^{t-i} \|\mathbf{r}(i) - \mathbf{W}(t)\mathbf{W}(t)^T \mathbf{r}(i)\|^2. \tag{4.23}$$

The idea in PASTd is to approximate $\mathbf{W}(t)^T\mathbf{r}(i)$ in (4.23), the unknown projection of $\mathbf{r}(i)$ onto the columns of $\mathbf{W}(t)$, by $\mathbf{y}(i) = \mathbf{W}(i-1)^T\mathbf{r}(i)$, which can be calculated for $1 \leq i \leq t$ at time t. This results in the following modified cost function

$$\tilde{J}[\mathbf{W}(t)] = \sum_{i=1}^{t} \beta^{t-i} \|\mathbf{r}(i) - \mathbf{W}(t)\mathbf{y}(i)\|^2. \tag{4.24}$$

The PASTd algorithm is based on the deflation technique which can be explained as follows. Firstly, minimizing (4.24) for $r = 1$, the most dominant eigenvector is calculated. Then the projection of the current data vector $\mathbf{r}(t)$ onto this most dominant eigenvector is removed from $\mathbf{r}(t)$ itself. Thus, the second most dominant eigenvector becomes the most dominant, and is calculated similarly. These steps are repeated till all the K most dominant eigenvectors are estimated.

The rank of the signal subspace, or equivalently the number of active users in the channel is estimated adaptively using information theoretic criteria as suggested in [5] such as Akaike information criterion (AIC) or minimum description length (MDL) both of which use the estimated eigenvalues.

Since in many problems in signal processing, the vector of observations can be modelled as a superposition of a finite number of signals with additive noise, estimating the number of signals in the observation vector has become a key issue. One approach for the solution to this problem is based on the observation that the number of signals can be determined from the eigenvalues of the covariance matrix of the observation vector. Methods developed by Bartlett [23] and Lawley [24] use a nested sequence of hypothesis tests that are based on this approach.

However, in this thesis, we use two similar methods which use a new approach to such problems and are based on the application of the information theoretic criteria for model selection introduced by Akaike [25, 26] and by Schwartz [27] and Rissanen [28]. These referred studies of Akaike introduce his pioneering work AIC whereas both Schwartz's and Rissanen's approaches yield the same criterion, MDL. The number of the signals is given with the value that minimizes the criteria AIC or MDL [29].

AIC and MDL are defined as follows

$$\mathrm{AIC}(k) \triangleq (N-k)L \ \ln\alpha(k) + k(2N-k) \tag{4.25}$$

$$\mathrm{MDL}(k) \triangleq (N-k)L \ \ln\alpha(k) + \frac{k}{2}(2N-k) \ \ln L \tag{4.26}$$

where L denotes the number of data samples used in the estimation. When an exponentially weighted window with forgetting factor β is applied to the data, the equivalent number of data samples is $L = 1/(1-\beta)$ where forgetting factor is chosen as $\beta = 0.995$ for simulations in this study. And $\alpha(k)$ above is defined as

$$\alpha(k) = \frac{\left(\sum_{i=k+1}^{N} \hat{\lambda}_i\right)/(N-k)}{\left(\prod_{i=k+1}^{N} \hat{\lambda}_i\right)^{1/(N-k)}} \tag{4.27}$$

The estimated rank of the signal subspace (that is the number of the signals in the observation vector) is the value k that minimizes (4.25) or (4.26). The summary of the PASTd algorithm is given in Table 4.1.

Table 4.1: PASTd Algorithm [5, 6]

Updating the eigenvalues and eigenvectors of signal subspace $\{\lambda_k,\ u_k\}_{k=1}^{K}$		
	$\mathbf{x}_1(t)$	$= \mathbf{r}(t)$
FOR	$k = 1 : K_t - 1$	
	$y_k(t)$	$= \mathbf{u}_k^H(t-1)\mathbf{x}_k(t)$
	$\lambda_k(t)$	$= \beta\lambda_k(t-1) + \lvert y_k(t)\rvert^2$
	$\mathbf{u}_k(t)$	$= \mathbf{u}_k(t-1) + [\mathbf{x}_k(t) - \mathbf{u}_k(t-1)y_k(t)]\, y_k(t)^*/\lambda_k(t)$
	$\mathbf{x}_{k+1}(t)$	$= \mathbf{x}_k(t) - \mathbf{u}_k(t)y_k(t)$
END		
	$\sigma^2(t)$	$= \beta\sigma^2(t-1) + \lVert\mathbf{x}_{K_{t-1}+1}(t)\rVert^2/(N-K_{t-1})$
Updating the rank of signal subspace K_t		
FOR	$k = 1 : K_t - 1$	
	$\alpha(k)$	$= \left[\sum_{i=k+1}^{N} \lambda_i(t)/(N-k)\right] / \left(\prod_{i=k+1}^{N} \lambda_i(t)\right)^{1/(N-k)}$
	$\mathrm{AIC}(k)$	$= (N-k)\ln[\alpha(k)]/(1-\beta) + k(2N-k)$
END		
	K_t	$= \arg\min_{0\le k\le N-1} \mathrm{AIC}(k) + 1$
IF	$K_t < K_{t-1}$	THEN
	remove	$\{\lambda_k(t), \mathbf{u}_k(t)\}_{k=K_t+1}^{K_{t-1}}$
ELSE IF	$K_t > K_{t-1}$	THEN
	$\mathbf{u}_{K_t}(t)$	$= \mathbf{x}_{K_{t-1}+1}(t)/\lVert\mathbf{x}_{K_{t-1}+1}(t)\rVert$
	$\lambda_{K_t}(t)$	$= \sigma^2(t)$
END		

The PASTd algorithm consists of two main parts. One is the computation of the eigen-components and the second is tracking the rank of the signal subspace. In

simulations, initial values are obtained by performing SVD for the first 50 data vectors.

4.3.3 Simulation Experiments with Rank-K MMSE Detector

4.3.3.1 The Case of AWGN Channel

Scenario-1: A synchronous CDMA system with $K = 6$ users using Walsh spreading codes with processing gain $N = 32$ is considered. User-1 is the desired user of SNR = 20 dB. There are four 10 dB multiple access interferers (MAIs) and one 20 dB MAI, i.e., $A_k^2/A_1^2 = 10$ for $k = 2, 3, 4, 5$, and $A_k^2/A_1^2 = 100$ for $k = 6$. The performance measure is the time averaged output signal-to-interference ratio (SIR) which is defined as $SIR = \mathrm{E}^2\{\mathbf{m}^T\mathbf{r}\}/Var\{\mathbf{m}^T\mathbf{r}\}$, where the expectation is with respect to the data bits of MAIs and the noise. In the simulations, the expectation operation is replaced by the time averaging operation as in [6]. The data plotted in figures are averaged over 1000 independent runs.

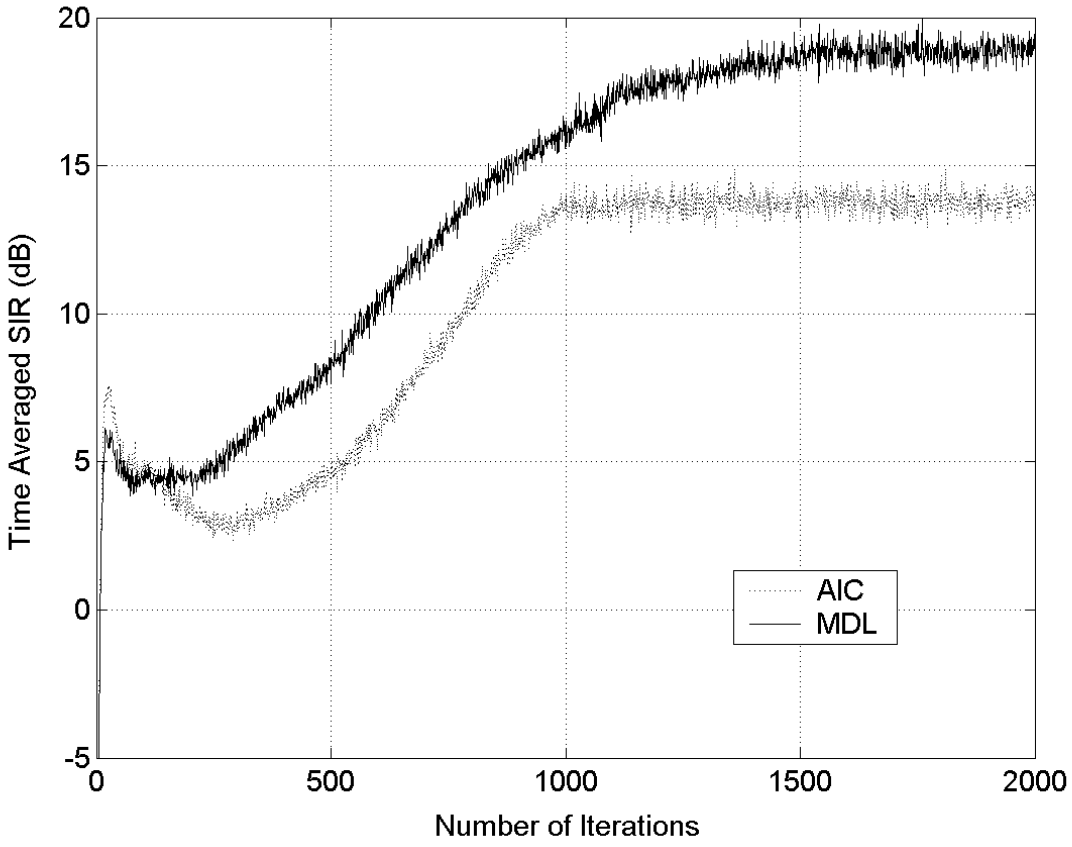

Figure 4.1: Time averaged SIR of the desired user with AIC and MDL in AWGN channel versus the iteration number. (Walsh spreading codes with N=32, K=6, SNR_1=20 dB; SNR_i=30 dB, $i = 2, 3, 4, 5$ SNR_6=40 dB. 1000 independent runs.)

Figure 4.1 shows the SIR performance of rank-K detector with AIC and MDL

as the information criterions used. For this scenario, the detector using MDL shows much better performance than the detector with AIC. Detector with MDL converges approximately to 18 dB SIR after 1500 iterations whereas detector with AIC converges to a SIR level of about 14 dB after 1000 iterations. Detector using MDL gives a better performance result than detector using AIC in the overall view for rank-K detector.

Furthermore, Figure 4.2 shows the subspace tracking capabilities of the same detector for the same scenario. The PASTd algorithm converges to the real signal subspace of rank-6, but a little slow as it is seen through the graphs. The rank tracking capability of MDL is seen to be better than that of the AIC about one subspace dimension.

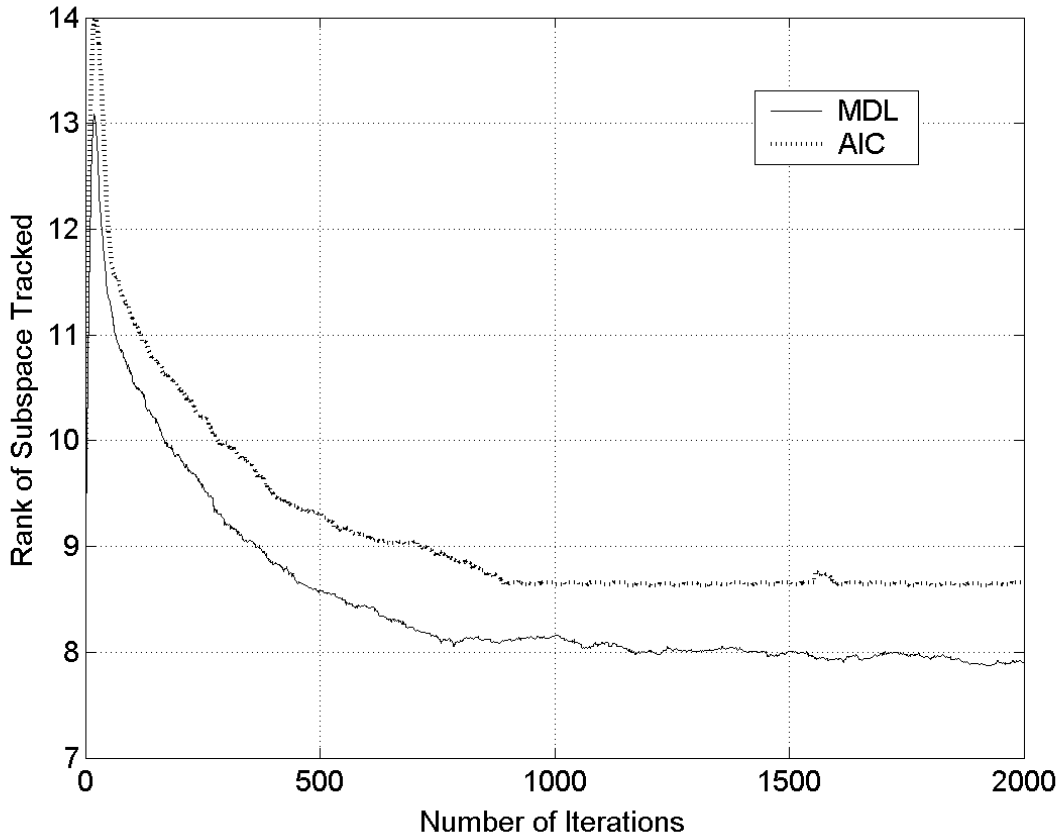

Figure 4.2: Estimated rank with AIC and MDL in AWGN channel versus the iteration number. (Walsh spreading codes with N=32, K=6, SNR_1=20 dB; SNR_i=30 dB, $i = 2, 3, 4, 5$ SNR_6=40 dB. 1000 independent runs.)

Scenario-2: In Figure 4.3 the simulation results of another scenario with the same synchronous CDMA system are plotted. This time simulation begins with six 10 dB MAIs (that is $\text{SNR}_i = 30dB,\ i = 2, \ldots, 7$). At t = 2000 two 20 dB MAIs ($\text{SNR}_i = 40dB,\ i = 8, 9$) enter the system and at t = 4000 the two 20 dB MAIs and four of the 10 dB MAIs exit. Desired user is again user-1 with SNR = 20 dB.

Since AIC and MDL gives similar results for this scenario with rank-K detector,

Figure 4.3 shows the performance with AIC as in [6]. Again, the response of the rank-K detector upon entering/exiting users is given by both SIR performance and rank-tracking ability.

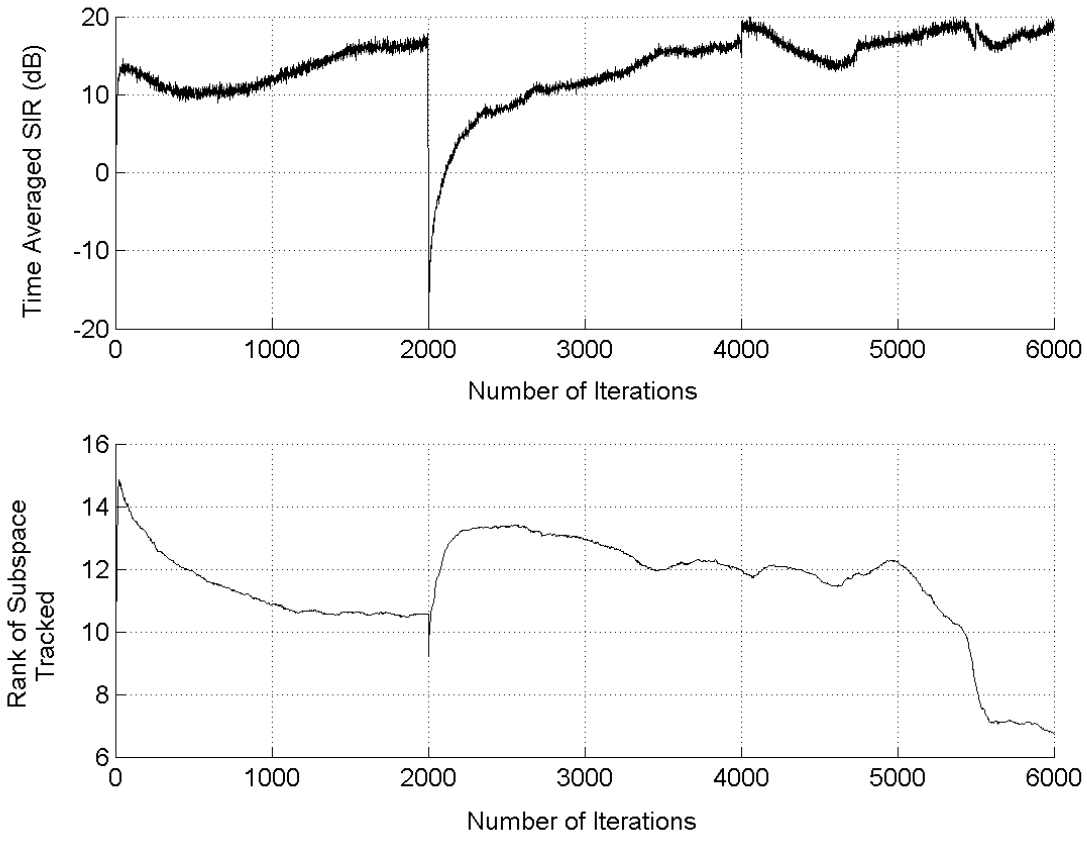

Figure 4.3: Time averaged SIR of the desired user and estimated rank versus the iteration number in the case of entering/exiting users. (Walsh spreading codes with N=32, beginning: six 10 dB MAIs, at t = 2000 two 20 dB MAIs enter, at t = 4000 two 20 dB MAIs and four of the 10 dB MAIs exit. SNR_1=20 dB. 1000 independent runs.)

From the beginning of the simulation till $t = 2000$, the detector acts as in Figure 4.1, because till then the system in *Scenario-2* is similar to *Scenario-1.* SIR value reaches the level of 16 dB. At $t = 2000$, with entering users the SIR value decreases till about -20 dB. After about 2000 iterations it reaches approximately 16 dB level again. At $t = 4000$, exiting users result in a slight performance gain. As in the lower graph in Figure 4.3, the rank tracking ability follows the response in SIR graph. Just after $t = 2000$ instant, the detector loses the tracked rank and begins searching and then converges again. With exiting users rank tracking becomes easier and faster.

4.3.3.2 The Case of Multipath Fading Channel with AWGN

Figures 4.4 and 4.5 show the averaged SIR and the rank of the tracked subspace

of the rank-K MMSE detector in a multipath channel.

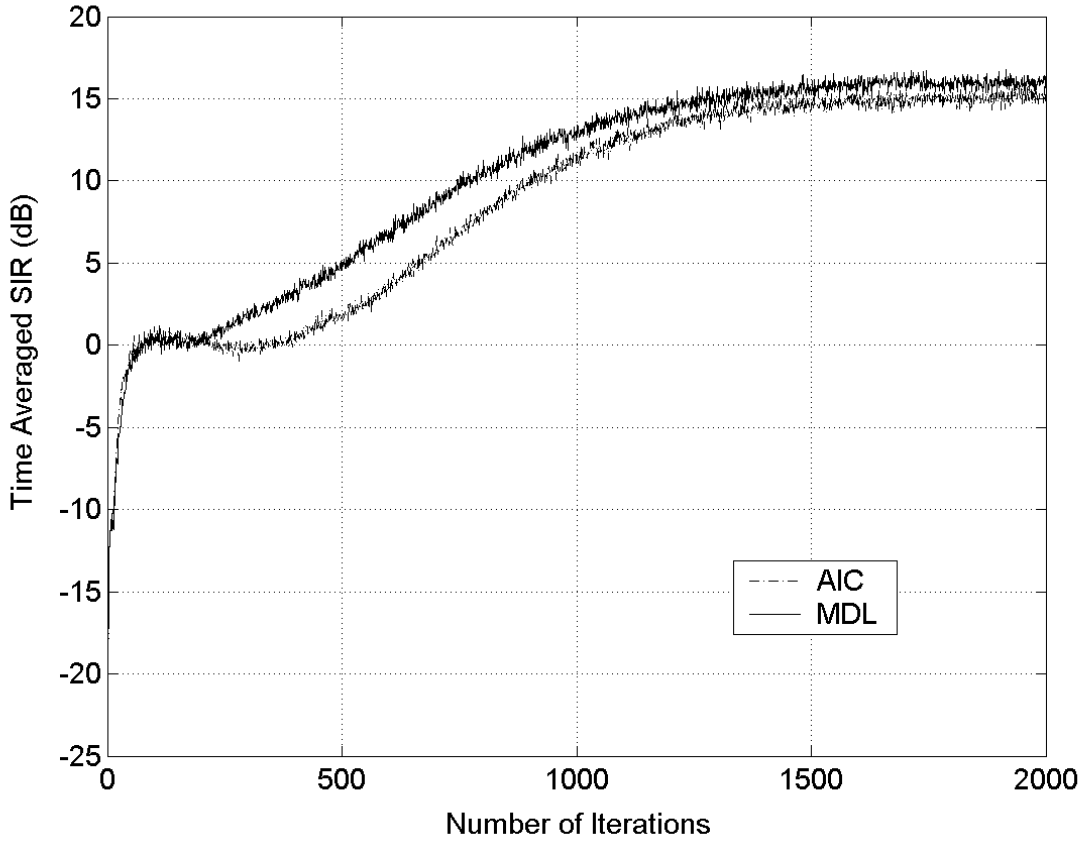

Figure 4.4: Time averaged SIR of the desired user with AIC and MDL in a multipath channel versus the iteration number. (Walsh spreading codes with N=32, K=6, SNR_1=20 dB; SNR_i=30 dB, $i = 2, 3, 4, 5$; SNR_6=40 dB. 1000 independent runs. Pedestrian A delay profile for IMT-2000 channels [30]. 1000 independent runs.)

The multipath channel is modelled with three taps, L = 3. Delay times are chosen as multiples of one chip interval, and power parameters are taken from [30] for Pedestrian A which are derived from physical tests on International Mobile Telecommunication 2000 (IMT-2000) channels. Properties of the system are as in *Scenario-1* again. The figures show the performances with both AIC and MDL information criteria.

After acting similarly at the beginning, from $t = 200$ on rank-K detector using MDL performs 3 or 4 dB better than the detector using AIC. About $t = 1200$, both SIR values get closer to each other with a difference about 1 dB. Then detector with AIC converges to 15 dB level whereas detector with MDL converges to about 16 dB level. As in Figure 4.2 MDL is closer to the real subspace rank than AIC, but this time with about 0.5 difference.

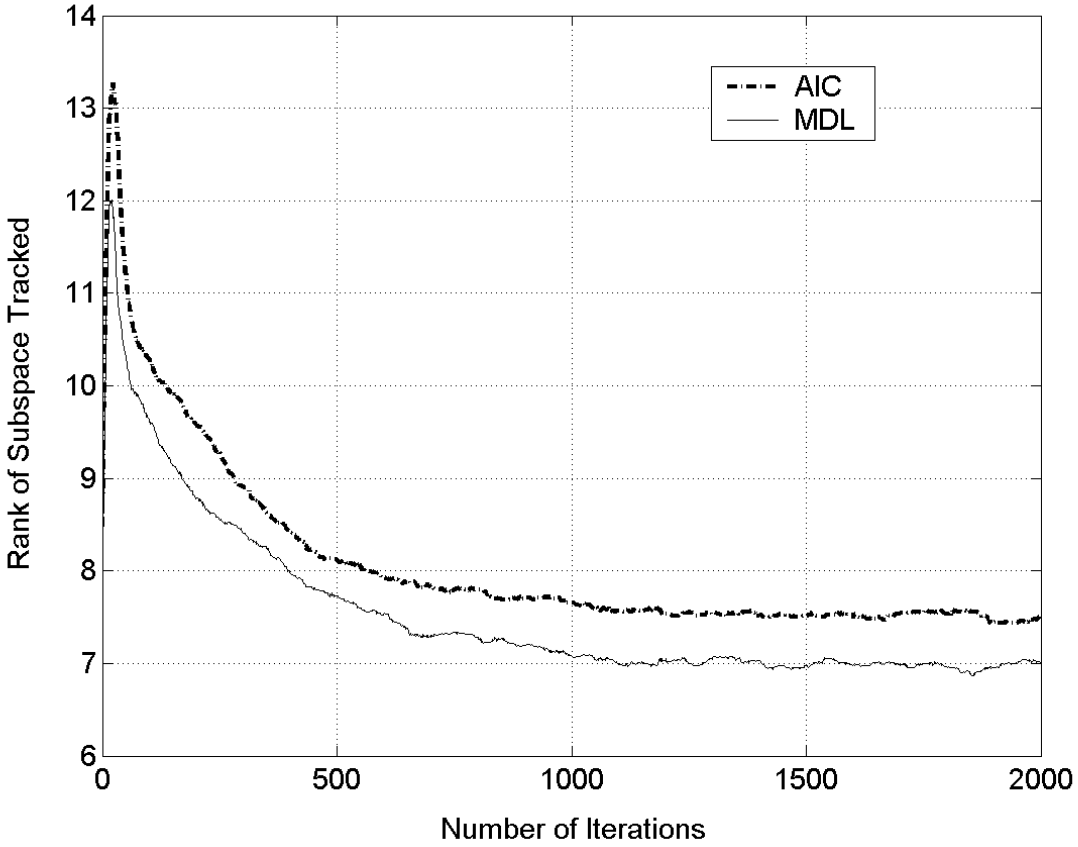

Figure 4.5: Estimated rank with AIC and MDL in a multipath channel versus the iteration number. (Walsh spreading codes with N=32, K=6, SNR_1=20 dB; SNR_i=30 dB, $i = 2, 3, 4, 5$; SNR_6=40 dB. 1000 independent runs. Pedestrian A delay profile for IMT-2000 channels [30]. 1000 independent runs.)

4.4 Reduced-Rank MMSE Detector

The idea in reduced-rank approach is to build a detector lying in a subspace of the signal space [8]. For reduced-rank MMSE detector we represent our detector by rewriting (4.20) in the following form

$$\mathbf{m}_r = \mathbf{U}_r \mathbf{\Lambda}_r^{-1} \mathbf{U}_r^T \mathbf{s}_1 \tag{4.28}$$

where we suppose that the matrix $\mathbf{U}_r$ contains r columns of $\mathbf{U}_s$ where $(r \leq K)$ and $\mathbf{\Lambda}_r$ consists of corresponding eigenvalues. And thus, the MSE in this case may be written as

$$\text{MSE}_r = 1 - \mathbf{s}_1^T \mathbf{U}_r \mathbf{\Lambda}_r^{-1} \mathbf{U}_r^T \mathbf{s}_1 \tag{4.29}$$

Proof [8]: Let $\boldsymbol{\omega} = [\omega_1, \omega_2, \ldots, \omega_r]^T$ and $\mathbf{m}_r = \mathbf{U}_r\, \boldsymbol{\omega}$. Then the MSE is calculated by

$$\begin{aligned} \text{MSE}_r &= E\{(b_1 - \mathbf{m}_r^T \mathbf{r})^2\}, \\ &= \mathbf{m}_r^T \mathbf{C}\ \mathbf{m}_r - 2\mathbf{m}_r^T \mathbf{s}_1 + 1, \\ &= \boldsymbol{\omega}^T \mathbf{U}_r^T \mathbf{C}\ \mathbf{U}_r\ \boldsymbol{\omega} - 2\,\boldsymbol{\omega}^T \mathbf{U}_r^T \mathbf{s}_1. \end{aligned} \tag{4.30}$$

Letting the derivative of MSE_r with respect to $\boldsymbol{\omega}$ be equal to $\mathbf{0}$ vector, we obtain $\boldsymbol{\omega}$ as

$$\frac{\partial(\text{MSE}_r)}{\partial\, \boldsymbol{\omega}} = 2\mathbf{U}_r^T \mathbf{C}\ \mathbf{U}_r\ \boldsymbol{\omega} - 2\mathbf{U}_r^T \mathbf{s}_1. \tag{4.31}$$

$$\boldsymbol{\omega} = (\mathbf{U}_r^T \mathbf{C}\ \mathbf{U}_r)^{-1} \mathbf{U}_r \mathbf{s}_1 = \boldsymbol{\Lambda}_r^{-1} \mathbf{U}_r \mathbf{s}_1 \tag{4.32}$$

Here, the fact that the eigenvectors are orthonormal, is used. The rank-r MMSE detector in (4.28) follows from (4.32). Substituting $\boldsymbol{\omega}$ in (4.32) into (4.30), we obtain the MSE in (4.29).

In order to choose the reduced-rank signal subspace, or equivalently $\mathbf{U}_r$, we define a quantity Q_i as

$$Q_i = \frac{\|\mathbf{s}_1^T \mathbf{u}_i\|^2}{\lambda_i} \tag{4.33}$$

where Q_i can be viewed as the normalized energy of user-1 projected onto the ith eigenvector. And MSE in (4.21) can be rewritten as

$$\text{MSE} = 1 - A_1^2 \sum_{i=1}^{K} Q_i. \tag{4.34}$$

It is seen from (4.34) that the optimal rank-r MMSE detector lies in the subspace spanned by the r eigenvectors corresponding to the r largest Q_i.

Of course, in practice, a mobile user will only know his own spreading code, but will not know the other users' codes. So, the auto-correlation matrix will be estimated from a limited number of data samples again, and the reduced-rank MMSE detector will be built on this estimated auto-correlation matrix, blindly.

4.4.1 Adaptive Reduced-Rank MMSE Detector With Subspace Tracking

Due to the similar reasons mentioned in the design of rank-K detector, for reduced-

rank MMSE detector, we again need to use an algorithm working in sample-by-sample fashion, instead of classical batch algorithms ED or SVD. We use for rank-r detector an algorithm named low-rank adaptive filter (LORAF1) introduced in [7]. Because PASTd algorithm has a slower convergence speed compared to the one of LORAF1 even though PASTd has a lower computational complexity of order NK ($O(NK)$) where N is the processing gain and K is the number of active users in the channel. Since, in CDMA systems, several users enter/exit the system, we need a faster converging algorithm to track the signal subspace faster.

Table 4.2: LORAF1 Algorithm [7, 8]

Initialization $\mathbf{U}_o = \mathbf{I}_N; \mathbf{\Theta}_0 = \mathbf{I}_N; \mathbf{A} = \mathbf{0}_N; K_0 = N-1; \beta = 0.995; \sigma^2 = 0; N_{\text{MSE}} = 10$		
Update $K_{t-1}+1$ eigenvectors in $\mathbf{U}_t$ and N eigenvalues $\{\lambda_i^t\}_{i=1}^N$		
	$\mathbf{z}_t$	$= \mathbf{U}_{t-1}^T \mathbf{r}_t$
	$\mathbf{A}_t$	$= \beta \mathbf{A}_{t-1} \mathbf{\Theta}_{t-1} + \mathbf{r}_t \mathbf{z}_t^T$
	$\mathbf{A}_t$	$= \mathbf{U}_t \mathbf{R}_t$: QR factorization
	$\mathbf{\Theta}_t$	$= \mathbf{U}_{t-1}^T \mathbf{U}_t$
	$\mathbf{x}$	$= \mathbf{r}_t - \mathbf{U}_t \mathbf{U}_t^T \mathbf{r}_t$
	σ_t^2	$= \beta \sigma_{t-1}^2 + \mathbf{x}^T \mathbf{x}/(N - K_{t-1} - 1)$
	$\{\lambda_k^t$	$= \mathbf{R}_t(k,k)\}_{k=1}^{K_{t-1}+1}$
	$\{\lambda_k^t$	$= \sigma_t^2\}_{k=K_{t-1}+2}^{N}$
Update the rank of signal space K_t		
FOR	$k = 1 : N-1$	
	$\alpha(k)$	$= \left[\sum_{i=k+1}^N \lambda_i^t/(N-k)\right] / \left(\prod_{i=k+1}^N \lambda_i^t\right)^{1/(N-k)}$
	AIC(k)	$= (N-k)\ln[\alpha(k)]/(1-\beta) + k(2N-k)$
END		
	K_t	$= \arg\min_{0 \le k \le N-1} AIC(k) + 1$
IF	$K_t < K_{t-1}$	THEN
	K_t	$= K_{t-1} - 1$
	$\mathbf{U}_t$	$= \mathbf{U}_t(:, 1 : K_{t-1})$
	$\mathbf{A}_t$	$= \mathbf{A}_t(:, 1 : K_{t-1})$
	$\mathbf{\Theta}_t$	$= \mathbf{\Theta}_t(1 : K_{t-1}, 1 : K_{t-1})$
ELSE IF	$K_t > K_{t-1}$	THEN
	$\mathbf{U}_t$	$= [\mathbf{U}_t,\ \mathbf{x}/\sigma^2]$
	$\mathbf{A}_t$	$= [\mathbf{A}_t,\ \mathbf{x}]$
	θ_t	$= \left[\begin{smallmatrix} \theta_t & \mathbf{0} \\ \mathbf{0} & 1 \end{smallmatrix}\right]$
END		

Furthermore, the optimal reduced-rank MMSE detector has been built using orthogonal eigenvectors which makes PASTd unsuitable for that detector since the basis vectors for the signal subspace tracked by PASTd are not orthogonal. Therefore, we use LORAF1 for reduced-rank MMSE detector, since it tracks orthogonal eigenvectors, faster. LORAF1 has computational complexity of $O(NK^2)$. Since the subspace tracking algorithm in LORAF1 cannot track the dimension of the signal subspace, the rank

tracking method mentioned in [5], which we have also used in rank-K detector is added to this algorithm. The final algorithm is given in Table 4.2.

LORAF1 can be divided into three main parts. In the first part, as in PASTd, eigen-components are computed. For this QR factorization is used. The second part tracks the signal subspace in a similar manner with PASTd. Here one of the information criterions, AIC or MDL is used. Finally, the rank of the signal subspace is reduced in a way that the desired user is included in. The quantity Q_i helps here to compute the reduced-rank. Initial values are chosen as given in Tables 4.2 and 4.3.

Table 4.3: LORAF1 Algorithm (rank reducing)[7, 8]

Choose the optimal reduced-rank MMSE detector c_0		
calculate $\{\hat{Q}_{i=1}^{K_t}\}$ and generate a matrix $\mathbf{V}$ whose first column $\mathbf{v}_1$ corresponds to the largest $\{\hat{Q}_{i=1}^{K_t}\}$ and second column $\mathbf{v}_2$ corresponds to the second largest $\{\hat{Q}_{i=1}^{K_t}\}$, and so on. Let η_i be the eigenvalue corresponding to $\mathbf{v}_i$		
	$\hat{\mathbf{c}}_0$	$= \mathbf{0}$
FOR $r = 1 : K_t$		
	$\hat{\mathbf{c}}_r$	$= \hat{\mathbf{c}}_{r-1} + \mathbf{v}_r \mathbf{v}_r^T \mathbf{p}/\eta_r$
	MSE(r)	$= 0$
FOR $i = 1 : N_{\text{MSE}}$		
	MSE(r)	$= \text{MSE}(r) + (\hat{b}_{t-i} - \hat{\mathbf{c}}_r^T \mathbf{r}_{t-i})^2$
END		
END		
	$\mathbf{c}_0$	$= \arg \min_{\{\hat{c}_r\}_{r=1}^{K_t}} \text{MSE}(r)$
	$\hat{b}_t$	$= sign(\mathbf{c}_0^T \mathbf{r}_t)$

4.4.2 Simulation Experiments with Rank-r MMSE Detector

4.4.2.1 The Case of AWGN Channel

For the first three figures, Figure 4.6, Figure 4.7 and Figure 4.8 the parameters of the system are chosen according to *Scenario-1* given in section 4.3.3.1.

Figure 4.6 and Figure 4.7 depict the simulation performance of the reduced-rank MMSE detector with the same curves as they are used in plotting the simulation results of rank-K MMSE detector in section 4.3.3, namely SIR and tracked rank of the subspace, respectively. Figure 4.8 added in this section shows the reduced-rank of the signal subspace as a function of iteration number.

As seen through the graphs, rank-r detector first tracks the signal subspace, then searches for a smaller subspace of the signal space where the desired user remains in. We see that rank tracking capabilities of AIC and MDL differ for this detector, too. MDL

overperforms AIC in tracking the signal space, this affects tracking the reduced-rank space, and so does the overall performance as seen with SIR graphs. So, we note here that MDL works better with rank-r detector than AIC, which is not mentioned in [8].

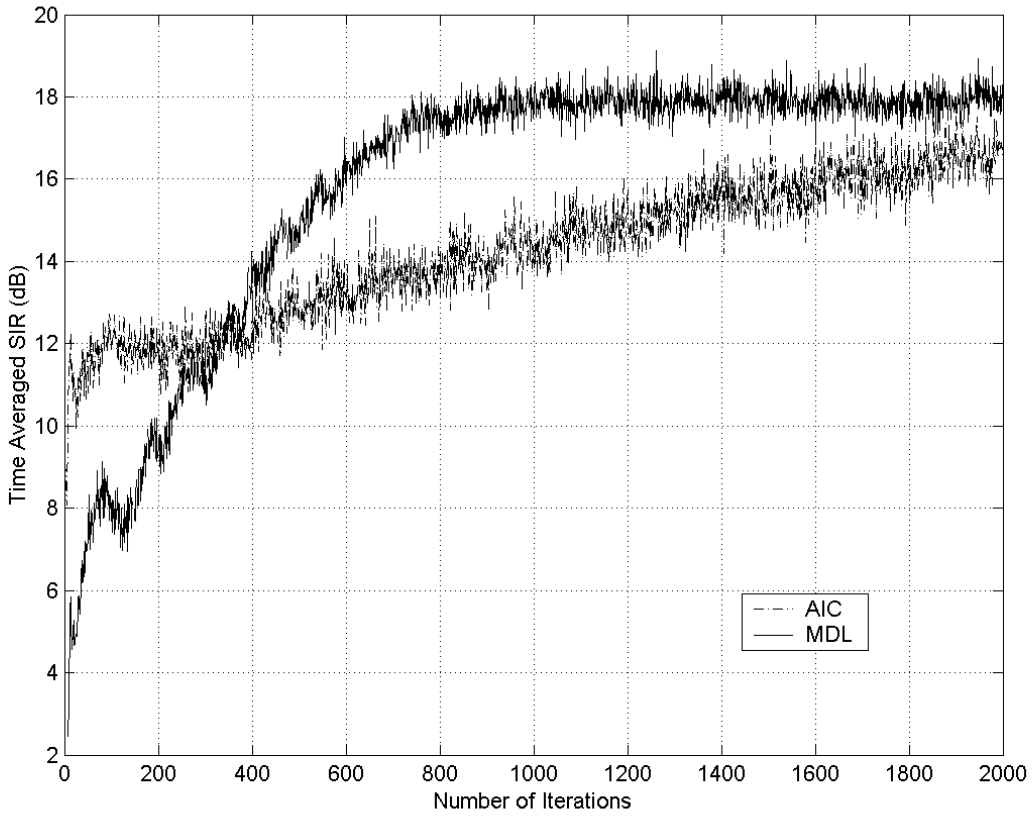

Figure 4.6: Time averaged SIR of the desired user with AIC and MDL in AWGN channel versus the iteration number. (Walsh spreading codes with N=32, K=6, SNR_1=20 dB; SNR_i=30 dB, $i = 2, 3, 4, 5$; SNR_6=40 dB. 1000 independent runs.)

Figure 4.6 depicts that although, rank-r detector using AIC reaches a higher SIR level during the first 300 iterations, rank-r detector using MDL converges to a level of 18 dB after 800 iterations. After 2000 iterations rank-r detector using AIC only reaches a level of 17 dB and it has still not converged.

Figures 4.9, 4.10 and 4.11 correspond to $Scenario - 2$ given in Section 4.3.3. Figures are plotted for both AIC and MDL comparing the average SIR performances, signal subspace rank and reduced-rank tracking behaviors, respectively.

Except the first adaptation period till $t = 2000$ both type of rank-r detectors using AIC and using MDL are seen to be very similar while adapting the entering or exiting users.

In Figures 4.10 and 4.11 tracked rank of signal subspace and the reduced-rank of signal subspace are given respectively. In Figure 4.10 we see that AIC and MDL behaves

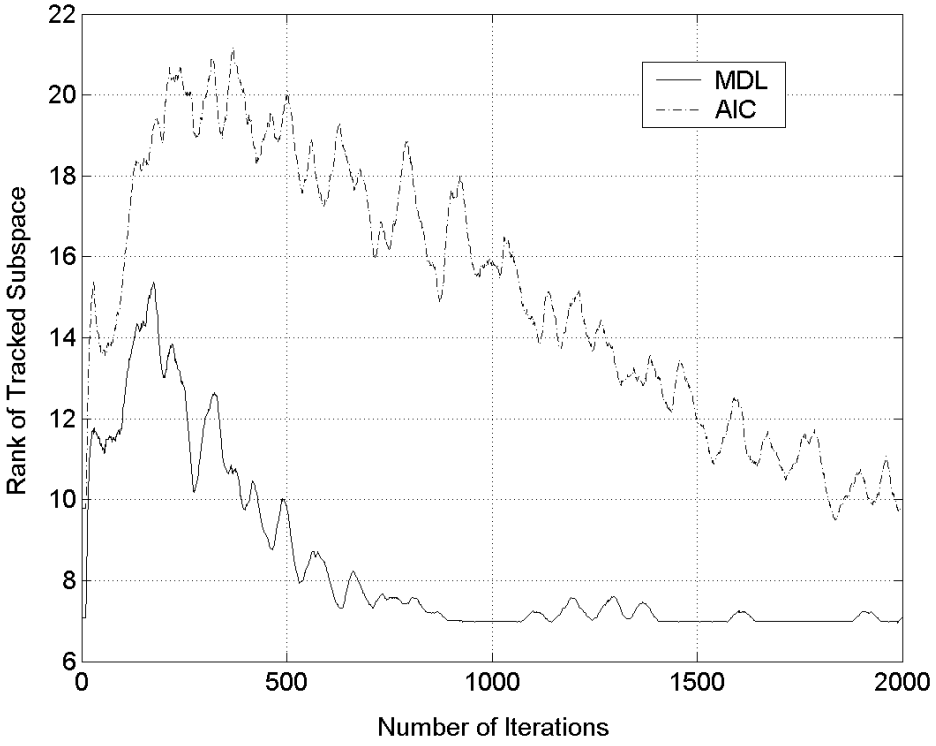

Figure 4.7: Estimated rank with AIC and MDL in AWGN channel versus the iteration number. (Walsh spreading codes with N=32, K=6, SNR_1=20 dB; SNR_i=30 dB, $i = 2, 3, 4, 5$; SNR_6=40 dB. 1000 independent runs.)

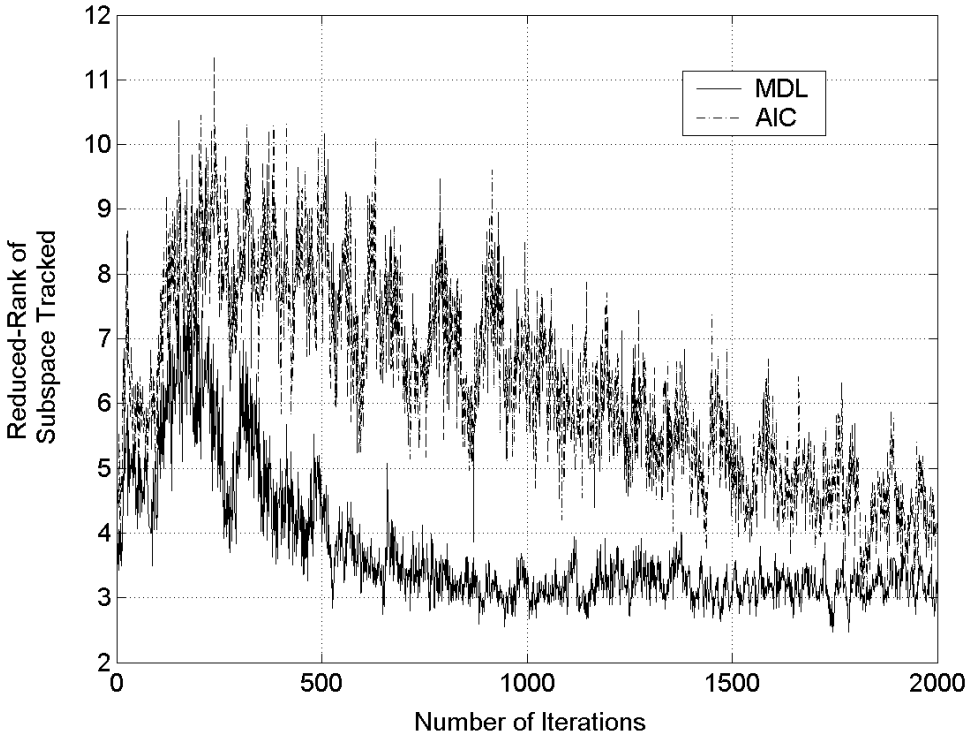

Figure 4.8: Estimated reduced-rank with AIC and MDL versus the iteration number. (Walsh spreading codes with N=32, K=6, SNR_1=20 dB; SNR_i=30 dB, $i = 2, 3, 4, 5$; SNR_6=40 dB. 1000 independent runs.)

very similar on tracking the subspace beginning with the 2000th iteration where two 40 dB users enter the system.

Note here that even the convergence takes at least 1000 iterations at the beginning, once the detectors track the signal subspace rank, they adapt themselves to changing channel conditions very fast. This may be observed in three of the figures for this scenario (4.9, 4.10 and 4.11) looking around 2000th and 4000th iterations.

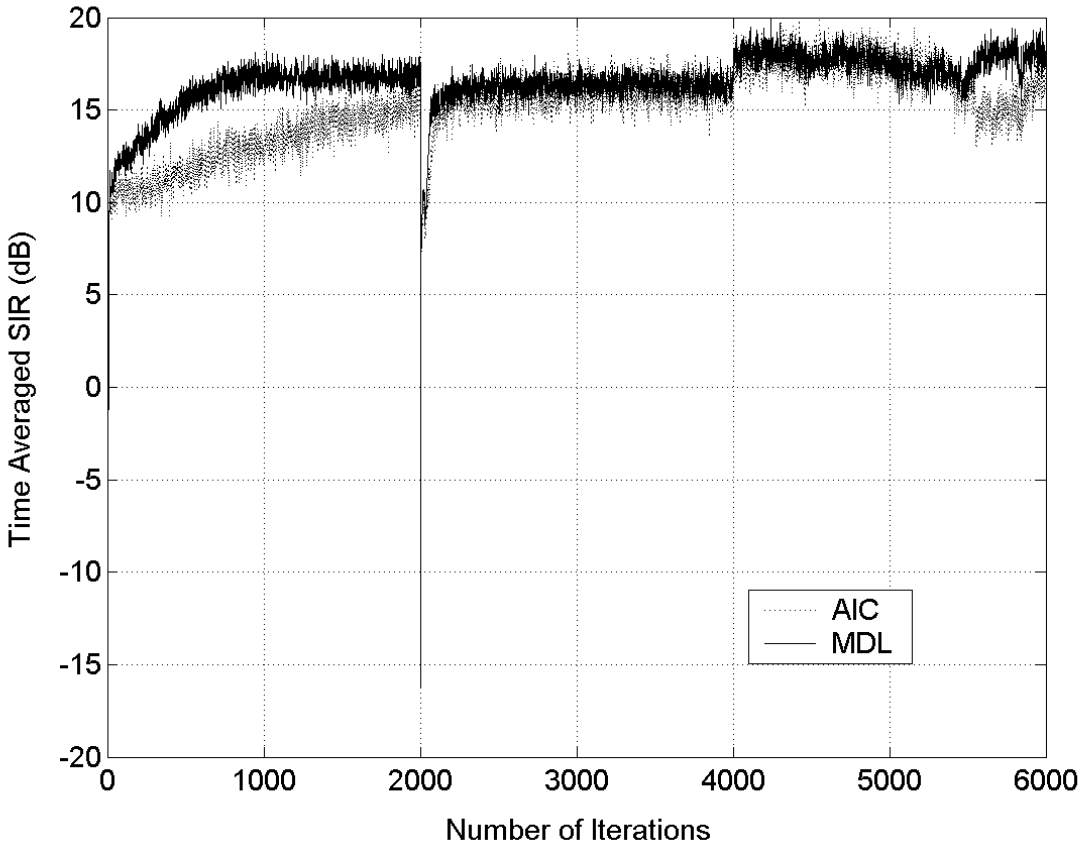

Figure 4.9: Time averaged SIR of the desired user and estimated rank versus the iteration number in the case of entering/exiting users. (Walsh spreading codes with N=32, beginning: six 10 dB MAIs, at t = 2000 two 20 dB MAIs enter, at t = 4000 two 20 dB MAIs and four of the 10 dB MAIs exit. SNR_1=20 dB. 1000 independent runs.)

4.4.2.2 The Case of Multipath Fading Channel with AWGN

The Figures 4.12, 4.13 and 4.14 show the performance of the reduced-rank MMSE detector in a multipath channel with information criterion as a parameter. The multipath channel is modelled again with three taps, L = 3. Delay times are chosen as a multiples of a chip period, and power parameters are taken from [30] for Pedestrian A which are derived from physical tests on IMT-2000 channels. Properties of the system are as in *Scenario-1* again.

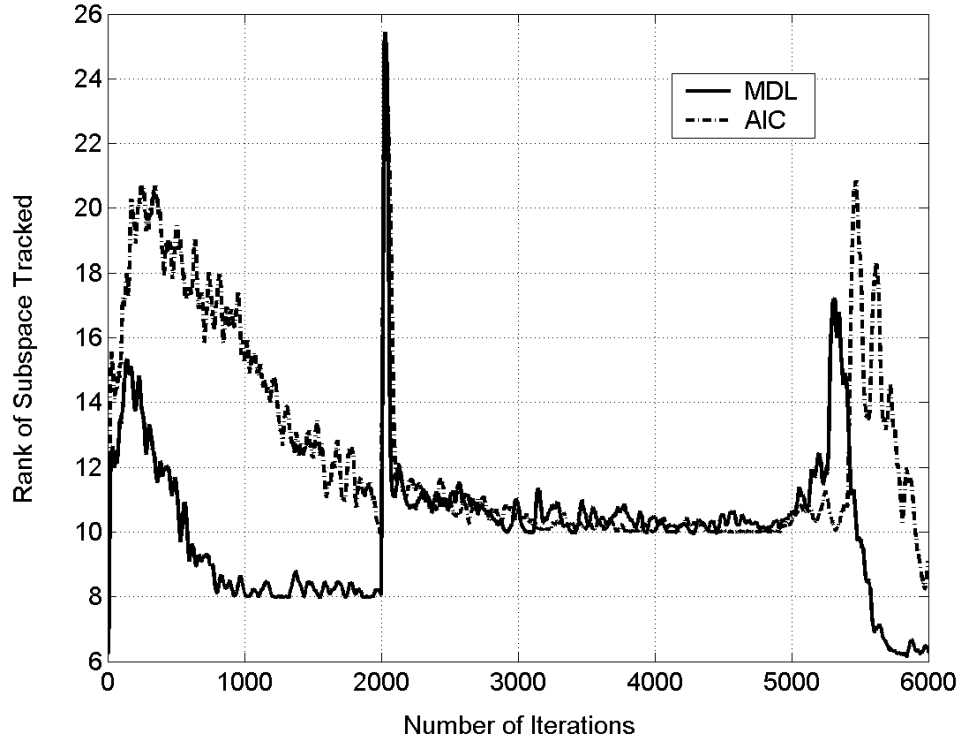

Figure 4.10: Estimated rank with AIC and MDL in AWGN channel versus the iteration number. (Walsh spreading codes with N=32, beginning: six 10 dB MAIs, at t = 2000 two 20 dB MAIs enter, at t = 4000 two 20 dB MAIs and four of the 10 dB MAIs exit. SNR_1=20 dB. 1000 independent runs.)

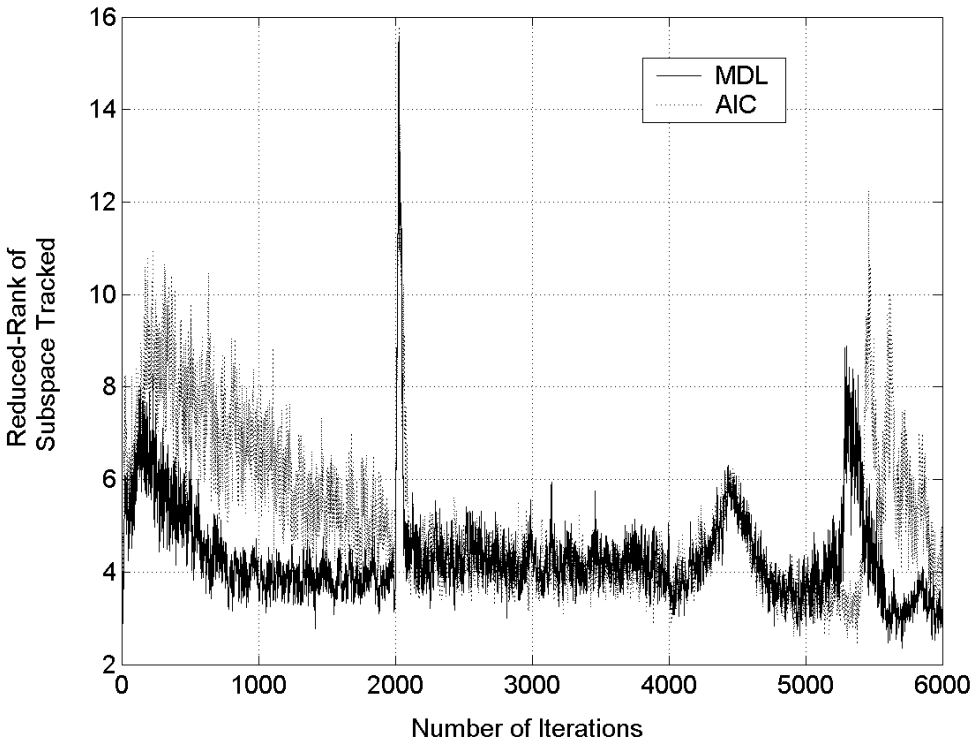

Figure 4.11: Estimated reduced-rank with AIC and MDL in AWGN channel versus the iteration number. (Walsh spreading codes with N=32, beginning: six 10 dB MAIs, at t = 2000 two 20 dB MAIs enter, at t = 4000 two 20 dB MAIs and four of the 10 dB MAIs exit. SNR_1=20 dB. 1000 independent runs.)

In Figure 4.12 it is seen that both SIR graphs, one for MDL and other for AIC differ beginning at about $t = 200$ and gather again at $t = 2000$. Between these two iteration levels the difference reaches nearly 8 dB at $t = 800$. Then they get closer till they intersect about 18 dB level at $t = 2000$. Rank-r detector with MDL converges this level at $t = 800$ whereas the other one using AIC at $t = 2000$.

The better performance of MDL to AIC is also seen in subspace tracking capabilities in Figure 4.13. Tracking the signal subspace rank better, MDL helps the detector to reduce this rank easier as it is seen in Figure 4.14.

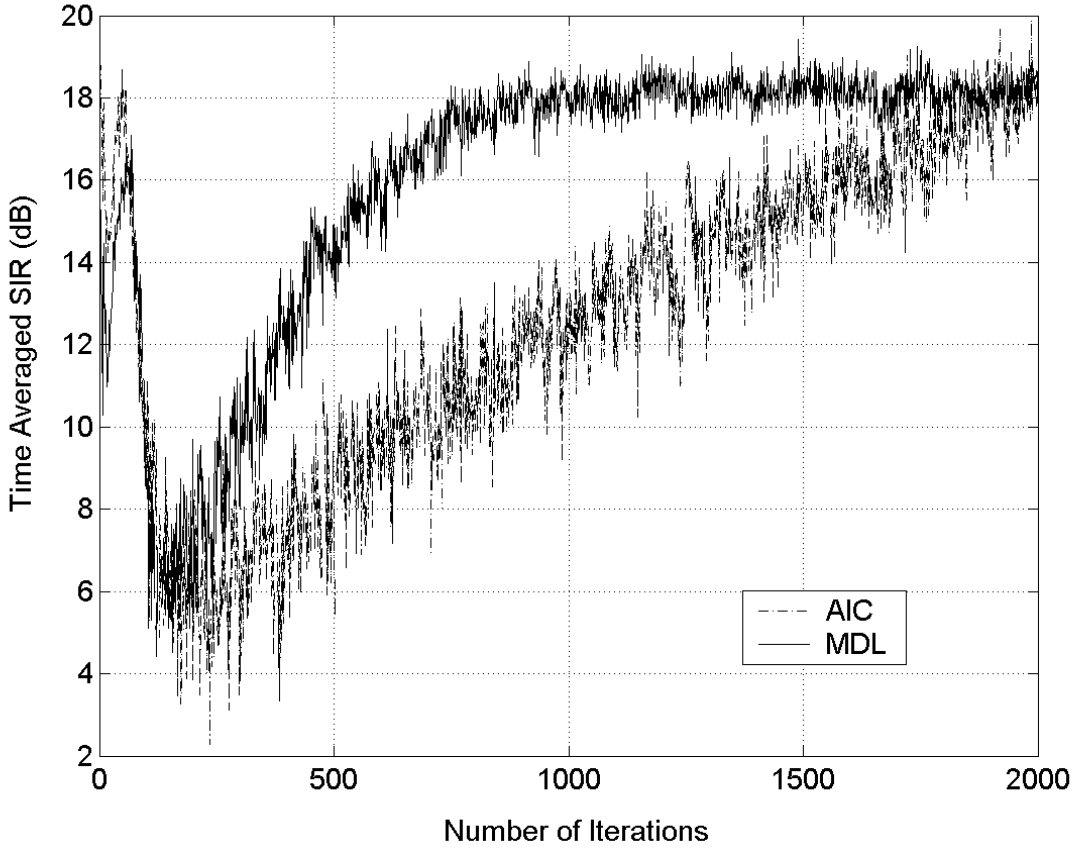

Figure 4.12: Time averaged SIR of the desired user with AIC and MDL in a multipath channel versus the iteration number. (Walsh spreading codes with N=32, K=6, SNR_1=20 dB; SNR_i=30 dB, $i = 2, 3, 4, 5$; SNR_6=40 dB. 1000 independent runs. Pedestrian A delay profile for IMT-2000 channels [30]. 1000 independent runs.)

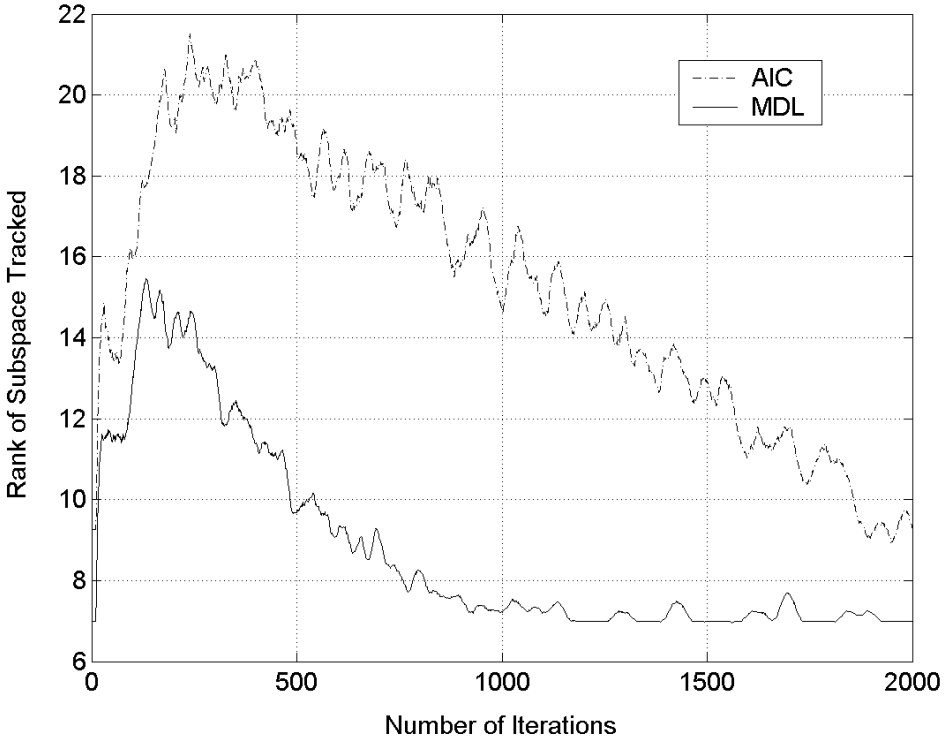

Figure 4.13: Estimated rank with AIC and MDL in a multipath channel versus the iteration number. (Walsh spreading codes with N=32, K=6, SNR_1=20 dB; SNR_i=30 dB, $i = 2, 3, 4, 5$; SNR_6=40 dB. 1000 independent runs. Pedestrian A delay profile for IMT-2000 channels [30]. 1000 independent runs.)

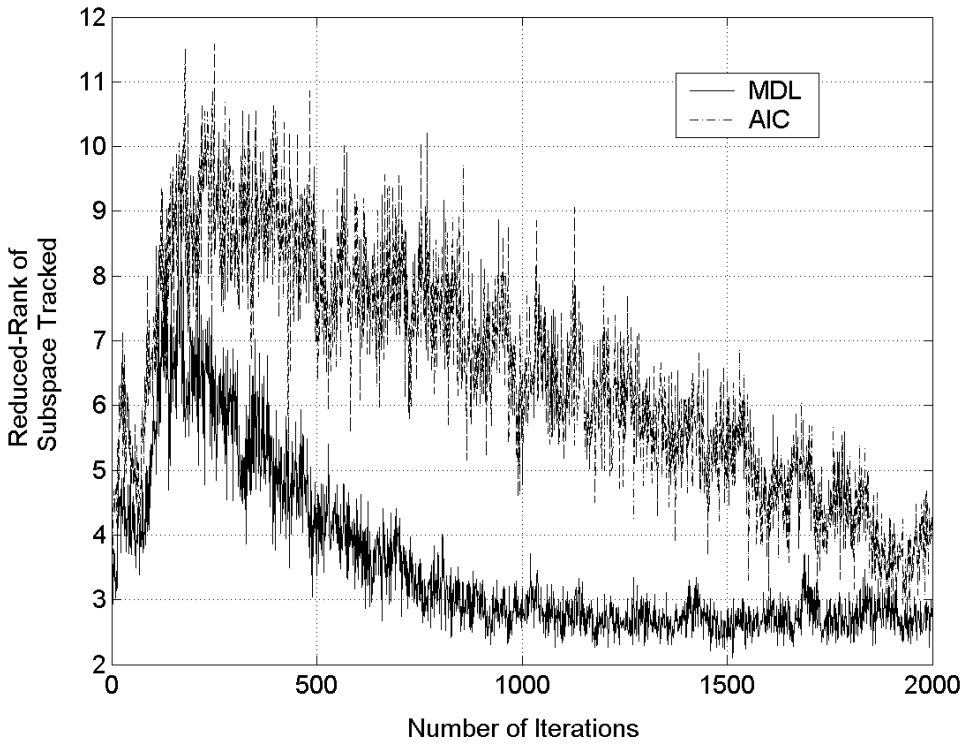

Figure 4.14: Estimated reduced-rank with AIC and MDL in a multipath channel versus the iteration number. (Walsh spreading codes with N=32, K=6, SNR_1=20 dB; SNR_i=30 dB, $i = 2, 3, 4, 5$; SNR_6=40 dB. 1000 independent runs. Pedestrian A delay profile for IMT-2000 channels [30]. 1000 independent runs.)

4.5 Performance Comparison of Rank-K and Rank-r MMSE Detectors

In this thesis, mostly, signal-to-interference ratio (SIR) is used as the performance criterion. In most cases the probability of error is very closely approximated by $\mathrm{Q}(\sqrt{\mathrm{SIR}})$ [16]. For this reason SIR is a meaningful criterion to compare the error probability performances of different algorithms. Therefore, following SIR comparisons of these two detectors also give an idea about their BER characteristics. An example for SIR and BER relation is given in Section 4.5.3 where BER characteristics of these two detectors are similar to their SIR characteristics for the AWGN channel given in this section in Figure 4.15. For further BER comparisons in different scenarios, SIR relations given in this section will also be a measure.

In this section comparison of two detectors, rank-K and reduced-rank (rank-r) detector, are given. For this, the simulation results above are brought together. Since through the previous simulations, MDL is seen to show better performance for both detectors, MDL is used for both rank-r and rank-K detectors.

4.5.1 The Case of AWGN Channel

Figure 4.15 corresponds to *Scenario-1* given in Section 4.3.3. The SIR of rank-r detector attains a value of approximately 18 dB after 800 iterations and till 1200th iteration it remains higher than the other. On the other hand, with lower SIR values until 1200th iteration rank-K detector converges to 19 dB level after then. Both SIR levels are very near to the ultimate limit of 20 dB given by the SNR of user-1.

In Figure 4.16 the SIR performances of the detectors in $Scenario-2$ given in section 4.3.3 are compared. Again, both detectors use MDL here.

The overall SIR performance of rank-r detector is superior to the one of rank-K detector. Furthermore, rank-r is more robust since its response to entering/exiting users is faster as mentioned in previous sections. Additionally, just after t = 2000, the estimates of the data bits would be mistaken with a higher percentage for rank-K detector. Its performance to entering users is not as good as its performance to exiting user and also not as good as the rank-r detector.

Figure 4.15 and Figure 4.16 prove the idea of rank-K and rank-r detectors, that is, since rank-K detector tracks the full rank signal subspace, its steady state SIR performance is better than rank-r detector as indicated in Figure 4.15. However, since the

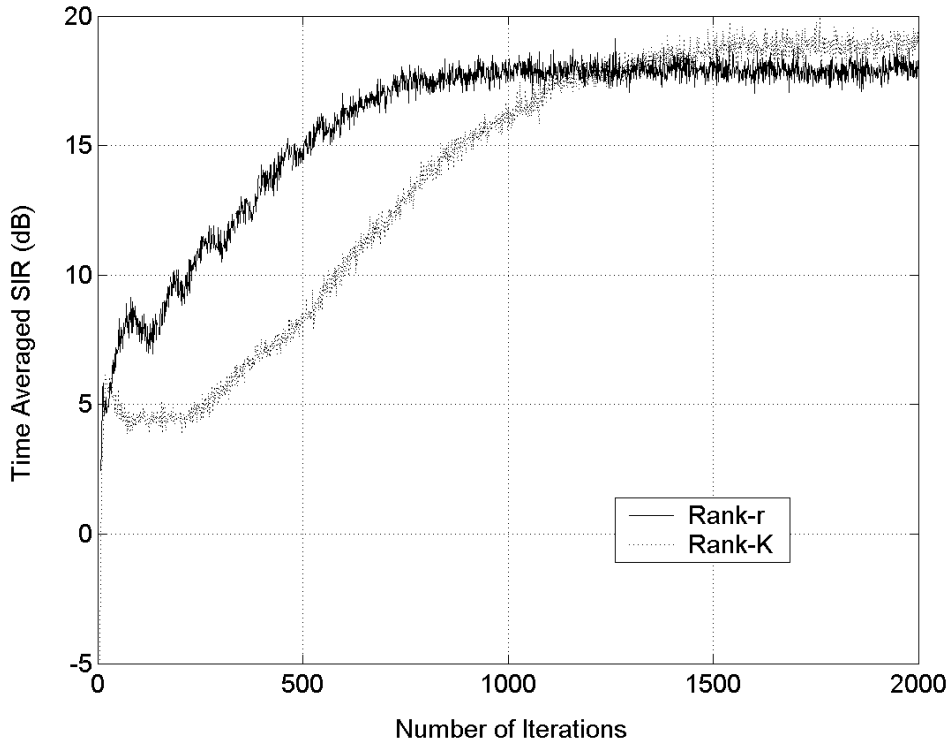

Figure 4.15: Time averaged SIR comparison of the desired user with rank-K and rank-r MMSE detectors in AWGN channel. (Walsh spreading codes with N=32, K=6, SNR_1=20 dB; SNR_i=30 dB, $i = 2, 3, 4, 5$; SNR_6=40 dB. 1000 independent runs.)

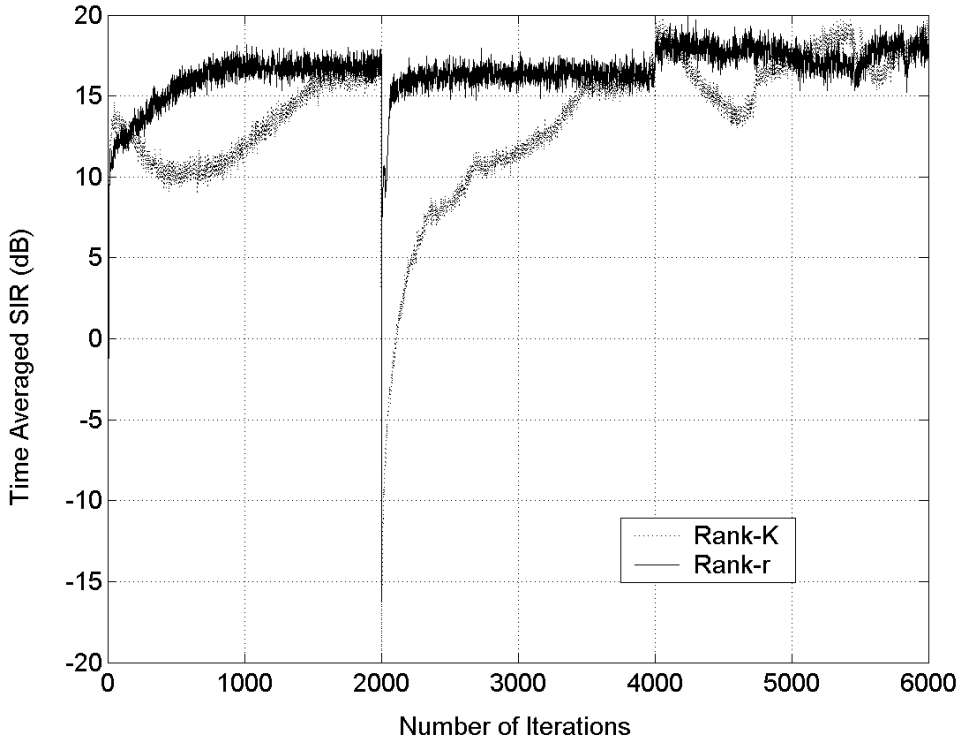

Figure 4.16: Time averaged SIR of the desired user comparison with rank-K and rank-r detectors in the case of entering/exiting users. (Walsh spreading codes with N=32, beginning: six 10 dB MAIs, at t = 2000 two 20 dB MAIs enter, at t = 4000 two 20 dB MAIs and four of the 10 dB MAIs exit. SNR_1=20 dB. 1000 independent runs.)

parameters to be estimated are less in number for rank-r detector, its convergence is faster than rank-K. Figure 4.16 depicts how convergence speed is important in a realistic channel. Therefore, in real life applications rank-r becomes a better alternative to rank-K detector with its higher convergence speed and acceptable SIR performance.

4.5.2 The Case of Multipath Fading Channel with AWGN

In Figure 4.17 the SIR performance of two detectors, namely rank-K and rank-r are compared in a fading multipath channel whose parameters are given before in section 4.3.3.

At the beginning of the iterations rank-K detector starts adapting with about a -15 dB average SIR value whereas the rank-r detector with an average SIR value of 15 dB. While rank-K detector converges 15 dB level at $t = 1500$, with a faster response rank-r detector reaches approximately 18 dB at $t = 1000$.

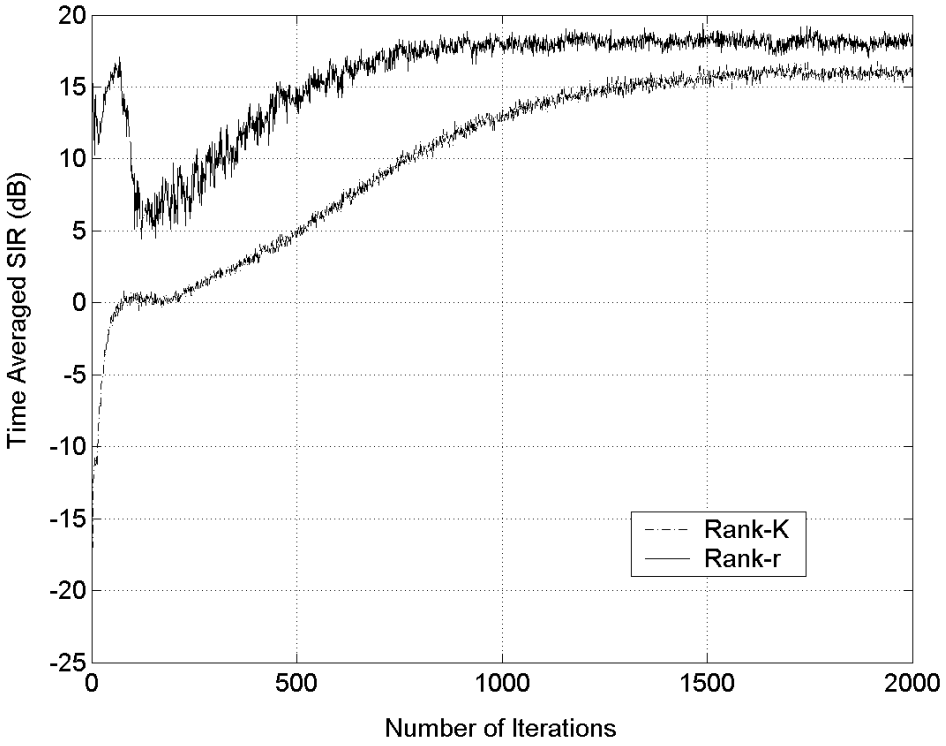

Figure 4.17: Time averaged SIR comparison of the desired user with rank-K and rank-r detectors in a multipath channel. (Walsh spreading codes with N=32, K=6, SNR_1=20 dB; SNR_i=30 dB, $i = 2, 3, 4, 5$; SNR_6=40 dB. 1000 independent runs. Pedestrian A delay profile for IMT-2000 channels [30]. 1000 independent runs.)

4.5.3 Comparison of BERs

In this section, BER performance comparison of five detectors, namely rank-K and rank-r, blind adaptive MMSE detectors with conventional and adaptive MMSE detectors and the batch algorithm JADE are plotted in Figure 4.18. For this comparison *Scenario-1* defined in Section 4.3.3 is used. Since for performing JADE, information of the number of users in the channel, K, and the whole data (transmitted bits) is required at the beginning, JADE performs very similar to the conventional MMSE mentioned in section 3.4. Beside this, adaptive MMSE that requires no information about signature codes but requires training sequences and timing of users gives worse but close performance results to JADE and conventional MMSE. They made no erroneous decision in 1000000 bit long simulations, more or less, after 5 dB SNR level. The BER performance of rank-r detector was better than all until about 0 dB SNR. As the SNR value increased rank-K detector performed slightly better than rank-r detector similar to the SIR behavior in Figure 4.15.

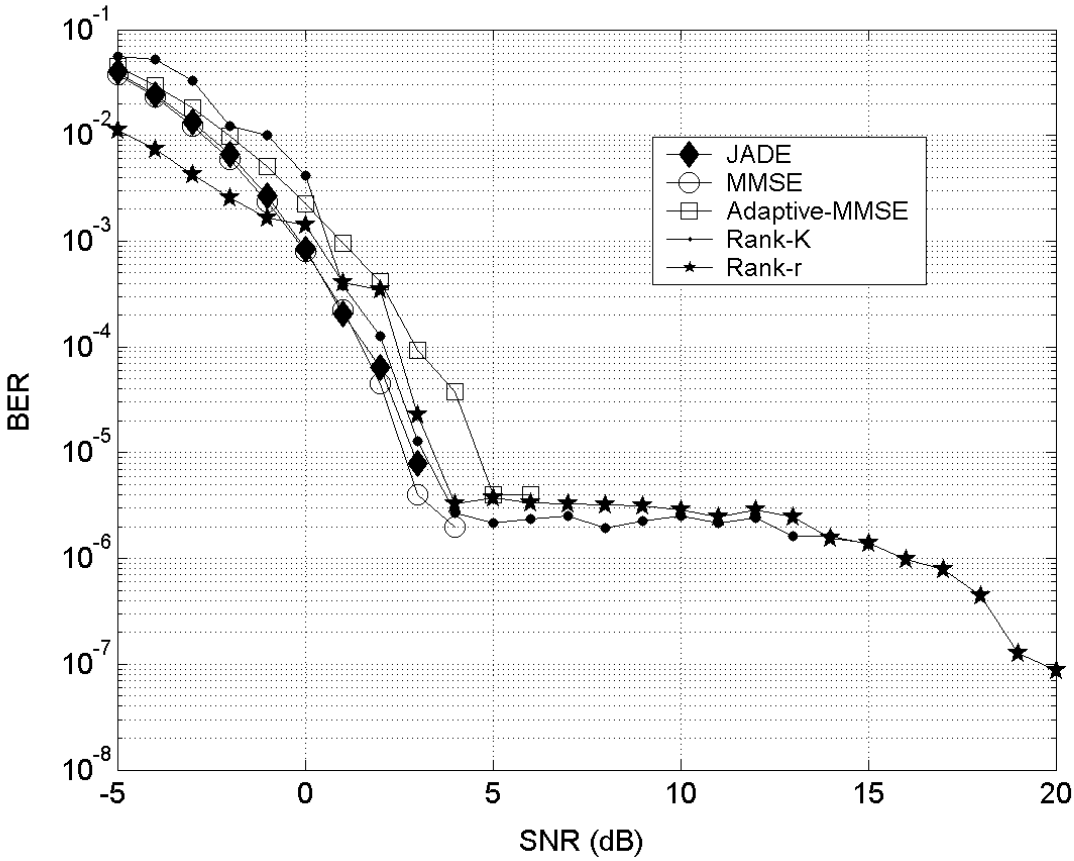

Figure 4.18: BER versus SNR comparison of JADE, MMSE, adaptive MMSE, rank-K and rank-r detectors in AWGN channel. (Walsh spreading codes with N=32, K=6, SNR_i=30 dB, $i = 2, 3, 4, 5$; SNR_6=40 dB.)

While commenting on this comparison the prior information requirements of those detectors should be taken into account. For example, while comparing blind detectors

JADE with rank-K and rank-r it should not be forgotten that rank-K and rank-r detectors work in a sample-by-sample fashion and both detectors track the signal subspace iteratively. However, JADE is given the whole data and the rank at the beginning.

According to this BER comparison rank-K and rank-r detectors are two powerful alternatives to others. Especially in conditions where the power of the desired user's signal is less than the power of the additive noise and at the same time when all interferers' SNRs are much higher, rank-r detector will be the best choice. Additionally, both rank-K and rank-r detectors provide such performances while remaining blind, just requiring the signature code of the desired user which is an important advantage.

Because of the fact that the BER curve can be closely approximated by the formula $\mathrm{Q}(\sqrt{(SIR)})$ [16], the simulated BER values for rank-K and rank-r detectors are computed with this formula using the asymptotic SIR value in the simulations, analytically.

CHAPTER 5

CONCLUSION

Multiuser detection techniques of CDMA communication are superior to single user detection in that they discriminate the signals of other users from the additive noise and try to eliminate their contribution in the demodulated signal in order to increase the noise margin of the detector. Additionally, subspace-based MUD methods emphasized in this thesis may be preferable to other batch methods because they work in a sample by sample fashion adaptively without requiring the whole data for performing the detection.

After introducing the rank-K detector which is defined by [6] and rank-r detector which is defined by [8], we have compared their performances. These comparisons were based on several scenarios defined for testing several abilities of the two detectors. Firstly, the performances were tested for an AWGN channel. One scenario was about a stable system in which the number of active users in the system is fixed during the simulation (*Scenario-1*). Secondly, we applied both detectors to a scenario where they had to track the changing rank of the signal subspace (*Scenario-2*). For the first scenario, SIR performance of rank-K detector reached a level about 1 dB higher than the other, but with a poor convergence speed. On the other hand, rank-r detector reached a very reasonable SIR level with a much higher convergence speed. For the second scenario, we made this comparison for a more realistic channel where rank-r detector remained as a preferable alternative to rank-K detector with its higher convergence speed and acceptable SIR performance related to its parameters to be estimated which are less in number than that of the rank-K detector.

Another performance comparison was done for a multipath channel which is a more realistic wireless channel. The parameters of the multipath channel which are taken from [30] where they are derived from measurement results for IMT-2000 systems. This comparison also showed the superiority of the rank-r detector with respect to the rank-K detector where similar behaviors as in the case of AWGN channel are observed.

All simulations for both detectors in [6] and in [8] were done by using Akaike information criterion (AIC) for tracking the rank of the signal subspace. In this thesis, we have also searched the performance with minimum description length (MDL) information criterion instead of AIC for both detectors. As a result, we have seen that MDL performed better than AIC for both detectors. This is a new remark not mentioned in [6] and [8],

and may be useful for further researches on the subject.

Finally, we compare the rank-K and the rank-r detectors with conventional and adaptive MMSE and batch type JADE detectors based on the BER performances. Upon this comparison, we may remind some notes here; JADE and conventional MMSE detectors perform very close to each other whereas the BER of adaptive MMSE detector is worse but very close to these previous two detectors. Rank-r detector performs best when the SNR level of the desired user is negative. As the SNR of the desired user is increased, BER of the rank-r detector becomes worse than the previous three but remains close to them. Rank-K detector gives the worst BER results when compared to others. As mentioned in the previous section, its BER performance increases only when the SNR of the desired user is greater than the MAIs' SNRs otherwise it remains still. As a result, when working fashions either batch or sample-by-sample and prior information requirements are taken into account rank-r (reduced-rank) detector seems to be a serious alternative to all other blind and non-blind detectors.

As advices for future works on the subject, we should mention a disadvantage of the reduced-rank blind adaptive MMSE detector. The most important one is the computational speed of the algorithm that is used for this detector. The rank adaptation algorithm of reduced-rank method is more computationally intensive compared to the one of the rank-K method. Since LORAF1 has a computational complexity of $O(NK^2)$, although its convergence speed is better, it is not as fast as PASTd of $O(NK)$, computationally. Some other algorithms may be searched for and tested with this detector in order to track orthogonal eigenvectors with faster computation speed. Since, the information criterion used with the algorithm clearly affects the capability and performance of the detectors other information criteria, or the way of using more than one criterion together may be searched.

REFERENCES

[1] J. G. Proakis, *Digital Communications*. USA:McGraw-Hill, 4th ed., 2001.

[2] M. Safak, *ELE 730 - Digital Communications 1 (Course Notes)*. Hacettepe University, Ankara, 1998.

[3] M. Karim and M. Sarraf, *W-CDMA and cdma2000 for 3G Mobile Networks*. USA: McGraw-Hill, 2002.

[4] I. Glover and P. Grant, *Digital Communications*. Great Britain: Prentice Hall Europe, 1998.

[5] B. Yang, "An extension of the pastd algorithm to both rank and subspace tracking," *IEEE Signal Processing Letters*, vol. 2, pp. 179–182, September 1995.

[6] X. Wang and V. H. Poor, "Blind mulituser detection: A subspace approach," *IEEE Transactions on Commununication*, vol. 49, pp. 1135–1141, July 2001.

[7] P. Strobach, "Low-rank adaptive filters," *IEEE Transactions on Signal Processing*, vol. 44, pp. 2932–2947, December 1996.

[8] H. G. Xiaodong Cai and A. N. Akansu, "Blind reduced-rank mmse detector for ds-cdma systems," *EURASIP Journal on Applied Signal Processing*, pp. 1365–1376, December 2002.

[9] E. S. IS-54-B, *Cellular System Dual-Mode Mobile Station-Base Station Compatibility Standard*. 1992.

[10] E. I. S. IS-136.2, *800 MHz TDMA-Radio Interface-Mobile Station-Base Station Compatibility-Traffic Channels and FSK Control Channels*. 1994.

[11] ETSI, *GSM Specifications 2.01, Version 4.2.0*. January 1993.

[12] ETSI, *GSM Specifications 2.01: Principles of Telecommunications Services*. January 1993.

[13] E. I. S. IS-95, *Mobile Station-Base Station Compatibility Standard for Dual-Mode Wideband Spread Spectrum Cellular System*. 1998.

[14] C. Andersson, *GPRS and 3G Wireless Applications*. USA: John Wiley and Sons, Inc., 2001.

[15] J. Glas, "Web site: http://cas.et.tudelft.nl/∼ glas."

[16] S. Verdu, *Multiuser Detection*. Cambridge, UK: Cambridge University Press, 1998.

[17] S. Lin and J. Daniel J. Castello, *Error Control Coding: Fundamentals and Applications*. New Jersey: Prentice Hall, 1983.

[18] S. B. Wicker, *Error Control Sytems for Digital Communication and Storage*. New Jersey: Prentice Hall, 1995.

[19] H. V. Poor, *An Introduction to Signal Detection and Estimation*. USA: Springer-Verlag, 2nd ed., 1994.

[20] J. Cardoso and A. Souloumiac, "Blind beamforming for non-gaussian signals," *IEE Proceedings-F*, vol. 140, pp. 362–370, December 1993.

[21] M. Feng and K. Kammeyer, "Blind source separation for communication signals using antenna arrays," *Proc. IEEE Int. Conference on Personal Wireless Communications(ICUPC-98), Florence, Italy*, October 1998.

[22] B. Yang, "Projection approximation subspace tracking," *IEEE Transactions on Signal Processing*, vol. 43, pp. 95–107, January 1995.

[23] M. S. Bartlett, "A note on the multiplying factors for various χ^2 approximations," *J. Roy. Stat. Soc.*, vol. 16, pp. 296–298, 1954.

[24] D. N. Lawley, "Tests of significance of the latent roots of the covariance and correlation matrices," *Biometrica*, vol. 43, pp. 128–136, 1956.

[25] H. Akaike, "Information theory and an extension of the maximum likelihood principle," *Proc. 2nd Int. Symp. Information Theory*, pp. 267–281, 1973.

[26] H. Akaike, "A new look at the statistical model identification," *IEEE Transactions on Automatic Control*, vol. AC-19, pp. 716–723, 1974.

[27] G. Schwartz, "Estimating the dimension of a model," *Ann. Stat.*, vol. 6, pp. 461–464, 1978.

[28] J. Rissanen, "Modelling by shortest data description," *Automatica*, vol. 14, pp. 465–471, 1978.

[29] M. Wax and T. Kailath, "Detection of signals by information theoretic criteria," *IEEE Trans. Acoust. Speech. Signal Processing*, vol. ASSP-33, pp. 387–392, April 1985.

[30] S. A. R. Michael Buehrer and A. Tonello, "Spatial channel model and measurements for imt-2000 systems," in *IEEE Vehicular Technology Conference, 2001*, vol. 1, pp. 342–346, 6-9 May 2001 VTC 2001 Spring.

APPENDIX A

TDMA(IS-136)

Table A.1: The IS-136 System Features

Multiple Access Scheme	TDMA
Spectrum Allocation	824 - 849 Mhz Uplink 869 - 894 Mhz Downlink
Channel Bandwidth	30 kHz
Modulation Data Rate on an RF Channel	48.6 kb/s
Modulation	$\pi/4$ - Shifted DQPSK
Number of Users per Channel	3 for full-rate speech and 6 for half-rate. There are 6 time slots / frame.
Digital Coding of Speech	Vector Sum Excited Linear Predictive coder (VSELP) at 7.95 kb/s with 159 bits per 20 ms frame.
Channel Coding	Combination of 7 - bit CRC and Convolutional Coding of rate 1/2.
User Data Transfer Capability	Limited capability, such as short messages on a dedicated control channel (DCCH)

APPENDIX B

GSM

Table B.1: GSM System Features

Multiple Access Scheme	TDMA
Spectrum Allocation	890 - 915 Mhz Uplink 935 - 960 Mhz Downlink
Channel Bandwidth	200 kHz
Modulation Data Rate on an RF Channel	270.8333 kb/s
Modulation	0.3 GMSK
Number of Users per Channel	8 for full-rate speech
Digital Coding of Speech	Regular pulse Excitation with Long-Term Predictor (RPE - LTP) at 13 kb/s for full-rate coding
Channel Coding	Combination of Block Coding and Convolutional Coding
User Data Transfer Capability	Circuit-switched data up to 12 kb/s and SMS

APPENDIX C

cdmaOne(Based on IS-95-A and IS-95-B)

Table C.1: cdmaOne System Features

Multiple Access Scheme	CDMA, FDD
Spectrum Allocation	Cellular CDMA: 824 - 849 MHz uplink 869 - 894 MHz downlink PCS CDMA: 1850 - 1910 MHz uplink 1930 - 1990 MHz downlink
Channel Bandwidth	1.23 MHz
Chip Rate	1.2288 Mb/s
Modulation(for Digital Data)	QPSK and OQPSK
Speech Coding	Code Excited Linear Predictive Coder (CELP) - 1.2, 2.4, 4.8, 9.6 kb/s for Cellular IS-95 and CELP - 14.4 kb/s for PCS IS-95
Number of Users per Channel	$\sim$16
User Data Transfer Capability	Packet data at 9.6 and 14.4 kb/s. In IS-95B, higher data rates may also be supported in steps of 8 kb/s.

APPENDIX D

3G System Features (UMTS and cdma2000)

Table D.1: UMTS and cdma2000 system Features

	W-CDMA(UTRA)	cdma2000
Multiple Access Scheme	FDD, TDD	FDD
Spectrum Allocation	FDD mode 1920 - 1980 MHz uplink 2110 - 2170 MHz downlink TDD mode 1900 - 1920 MHz 2010 - 2025 MHz	1850 - 1910 MHz uplink 1930 - 1990 MHz downlink
Channel Bandwidth	5 MHz	1.25 X N MHz. In initially, N may be 1, 2,or 3, but later could be 6, 9,or 12.
Chip Rate	3.84 Mc/s	1.2288 X N Mc/s
Frame Structure	10 ms	20 ms
Modulation (for Digital Data)	QPSK	QPSK
Speech Coding	Adaptive Multirate (AMR) Coding	AMR
User Data Transfer Capability	circuit mode: up to 144, 384 kb/s and 2.048 Mb/s packet mode: at least 144, 384 kb/s, and 2048 kb/s	144, 384, 2048 kb/s
3G Network Interface	GSM MAP (evolved version)	ANSI-41 (evolved version)